

Turbulence and Particle Acceleration in Giant Radio Haloes: the Origin of Seed Electrons

Anders Pinzke^{1,2*}, S. Peng Oh^{3*}, and Christoph Pfrommer^{4*}

¹*The Oskar Klein Centre for Cosmoparticle Physics, Stockholm University, AlbaNova University Center, SE - 106 91 Stockholm, Sweden*

²*Dark Cosmology Center, University of Copenhagen, Juliane Maries Vej 30, DK-2100 Copenhagen, Denmark*

³*University of California - Santa Barbara, Department of Physics, CA 93106-9530, USA*

⁴*Heidelberg Institute for Theoretical Studies (HITS), Schloss-Wolfsbrunnengasse 35, 69118 Heidelberg, Germany*

17 October 2018

ABSTRACT

About 1/3 of X-ray-luminous clusters show smooth, Mpc-scale radio emission, known as giant radio haloes. One promising model for radio haloes is Fermi-II acceleration of seed relativistic electrons by compressible turbulence. The origin of these seed electrons has never been fully explored. Here, we integrate the Fokker-Planck equation of the cosmic ray (CR) electron and proton distributions when post-processing cosmological simulations of cluster formation, and confront them with radio surface brightness and spectral data of Coma. For standard assumptions, structure formation shocks lead to a seed electron population which produces too centrally concentrated radio emission. Matching observations requires modifying properties of the CR population (rapid streaming; enhanced CR electron acceleration at shocks) or turbulence (increasing turbulent-to-thermal energy density with radius), but at the expense of fine-tuning. In a parameter study, we find that radio properties are exponentially sensitive to the amplitude of turbulence, which is inconsistent with small scatter in scaling relations. This sensitivity is removed if we relate the acceleration time to the turbulent dissipation time. In this case, turbulence above a threshold value provides a fixed amount of amplification; observations could thus potentially constrain the unknown CR seed population. To obtain sufficient acceleration, the turbulent magneto-hydrodynamics cascade has to terminate by transit time damping on CRs, i.e., thermal particles must be scattered by plasma instabilities. Understanding the small scatter in radio halo scaling relations may provide a rich source of insight on plasma processes in clusters.

Key words: acceleration of particles, cosmic rays, turbulence, gamma-rays: galaxies: clusters, radiation mechanisms: non-thermal, galaxies: clusters: general

1 INTRODUCTION

About one third of X-ray-luminous clusters show smooth, unpolarised radio emission on \sim Mpc scales, known as giant radio haloes (RHs) (Brunetti & Jones 2014). They appear only in disturbed, merging clusters and the RH luminosity correlates with the X-ray luminosity (Govoni et al. 2001; Feretti et al. 2012) and the Compton y -parameter (Basu 2012; Planck Collaboration et al. 2013). The RHs show that CR electrons and magnetic fields permeate a large volume fraction of the intra-cluster medium (ICM). The dominant CR source, given the smoothness and enormous extent of RHs, is thought to be structure formation shocks (Miniati et al. 2001a; Pfrommer 2008). At the same time,

plasma processes, the origin of magnetic fields and particle acceleration in a turbulent, high- β plasma (in which the thermal pressure predominates the magnetic pressure) like the ICM are not well understood. Radio haloes thus provide an incisive probe of non-thermal processes in the ICM.

There have been two competing models proposed to explain RHs. The radio emitting electrons in the “hadronic model” are produced in inelastic (hadronic) CR proton interactions with protons of the ambient thermal ICM, which generates pions that eventually decay into electrons and positrons, depending of the charge of the initial pion (Dennison 1980; Blasi & Colafrancesco 1999; Miniati et al. 2001b; Pfrommer & Enßlin 2004; Pfrommer et al. 2008; Enßlin et al. 2011). CR protons and heavier nuclei may have been accelerated and injected into the ICM by structure formation shocks, active galactic nuclei and galactic winds. However, the strong bimodality that separates X-ray lumi-

* apinzke@fysik.su.se (AP); peng@physics.ucsb.edu (SPO); christoph.pfrommer@h-its.org (CP)

nous clusters into radio-active and radio-quiet clusters (requiring a fast switch on/off mechanism of the RH emission) and the very extended RH emission at low frequencies in Coma (352 MHz) represent a major challenge to this model class (Brunetti et al. 2012; Zandanel et al. 2014).

The alternative model for RHs is re-energisation of seed suprathermal electrons by Fermi II acceleration when ICM turbulence becomes transsonic during mergers (Schlickeiser et al. 1987; Giovannini et al. 1993; Brunetti et al. 2001, 2004; Brunetti & Lazarian 2007, 2011; Miniati 2015). Due to the short radiative cooling time of high-energy relativistic electrons, the cluster synchrotron emission quickly fades away after a merger, which naturally explains the observed bimodality of RHs (see e.g. Donnert et al. 2013; Donnert & Brunetti 2014).

However, there is a salient piece missing in the turbulent reacceleration model. It relies heavily on the assumption of an abundant, volume-filling population of seed suprathermal electrons; direct Fermi II acceleration from the thermal pool is precluded by strong Coulomb losses (Petrosian & East 2008; Chernyshov et al. 2012). These seeds are presumed to be either fossil CR electrons (CRes) accelerated by diffusive shock acceleration (DSA) during structure formation (Sarazin 1999), or secondaries injected by hadronic interaction of CR protons (CRps) with thermal protons (Brunetti & Lazarian 2011).

While analytic estimates have been made, there has been no *ab initio* demonstration that structure formation can lead to the required abundance of seed electrons with the correct spatial and spectral characteristics. This is a non-trivial requirement: Coulomb cooling in dense cluster cores is severe, and DSA fossil electrons may not survive. On the other hand, for secondaries to constitute the seed population, the CRp population required in the best-studied case of the Coma cluster must have a very broad and flat (or even slightly inverted) spatial profile (Brunetti et al. 2012), in contrast with the thermal plasma whose energy density declines steeply with radius. In Figure 1 we show that such a distribution is not predicted by cosmological simulations (see also Pinzke & Pfrommer 2010; Vazza et al. 2014). If CRps are predominantly advected with the cluster plasma, their distribution will be peaked towards the cluster centre and show a similar characteristics as the thermal plasma. As a consequence, the distribution of secondary electrons and the resulting radio synchrotron emission is also peaked since the hadronic reaction is a two-body scattering process. Hence, the simulated emission falls short of the observed extended and flat radio profile of the Coma cluster.

Indeed, arriving at a seed population with the required characteristics is highly constraining, and has the potential to teach us much about the origin of CRps/CRes in clusters. In this work, we use our hydrodynamical zoom simulations of galaxy clusters in a cosmological setting to follow the distribution functions of seed populations for CRps and CRes, and integrate the Fokker-Planck equation of CR transport along Lagrangian particle trajectories. We model diffusive shock acceleration at structure formation shocks, and account for various loss processes of CRs. Utilising new insights from our recent work on DSA generated fossil electrons (Pinzke et al. 2013), we generate the first quantitative calculation of primary and secondary seed electrons.

To compare this to observations, we model second-order

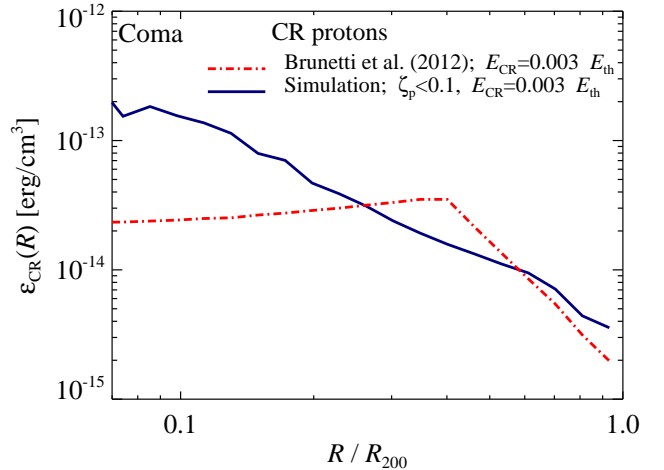


Figure 1. Spatial distribution of CRp energy density in the Coma cluster. The red dash-dotted line shows the required distribution of seed CRps that generate secondary electrons via proton-proton (p-p) collisions required to reproduce Coma radio brightness observations after Fermi-II reacceleration (Brunetti et al. 2012). The blue solid line shows the distribution of fossil CRps found in cosmological simulations, which disagrees with the required profile. To better compare the two models in this figure, we normalise the required distribution of CRps by fixing the total CRp energy E_{CR} to 0.3 per cent of the total thermal energy, consistent with observations (Ackermann et al. 2014; Arlen et al. 2012).

Fermi acceleration by CR interactions with magnetised turbulence. However, we assume a simplified and stationary model for magnetic fields and turbulence. We do not account for the time-varying energy density in compressible waves, which are thought to be necessary for the acceleration process (Brunetti & Lazarian 2007, 2011), as the cluster merger proceeds. So our approach is orthogonal (and complementary) to e.g., simulations of Miniati 2015 that focus on the time-dependent compressible turbulence while adopting a simplified treatment of CR. Our approach of parametrizing turbulence enables us to vary parameters associated with the spatial profile and the overall amplitude of compressible waves (that can in principle vary depending on the details of a particular cluster merger).

In this paper, we explore how the radio surface brightness profile and spectrum of the best known radio halo, Coma, can be used to constrain the underlying properties of the seed CRs and turbulence. We aim to constrain the normalisation and spatial profile of these two input ingredients in turbulent reacceleration models. The outline of this paper is as follows. In Section 2, we outline the basic physics of turbulent reacceleration of CRs which we use. In Section 3, we use cosmological simulations to generate a seed CR population, and combine it with our parametrized model of turbulence to produce radio surface brightness profiles and spectra of Coma. We find that it is possible to fit the observations using physically motivated modifications of the seed population (rapid streaming; enhanced CR electron acceleration at shocks) or turbulence (increasing the turbulent-to-thermal energy density, $\varepsilon_{\text{turb}}/\varepsilon_{\text{th}}$ with radius), but only at the expense of fine tuning. In Section 4, we explore the reason for this fine-tuning, and seek ways to overcome it. We

perform a parameter study on spherically symmetric, static models where we vary properties of the seed population and turbulence. We find exponential sensitivity to the amount of turbulence, which can be eliminated if the turbulent acceleration and dissipation time are linked. In this case, turbulence above a threshold value required to overcome cooling provides a fixed amount of amplification; observations could then potentially constrain the unknown CR seed population. We summarise and conclude in Section 5.

2 COSMIC RAY TRANSPORT

The transport of relativistic electrons and protons across cosmic time into galaxy clusters is a complex problem that depends on the velocity field of the gas (and its thermodynamic properties such as density, temperature, and pressure) as well as non-thermal processes (turbulence, magnetic fields, fossil CRs). We use high resolution galaxy cluster simulations to derive the thermal and fossil CR properties (shock accelerated primary CRs and CRps, as well as secondary CRs produced in p-p collisions, see Pfrommer et al. 2007; Pfrommer 2008; Pinzke & Pfrommer 2010; Pinzke et al. 2013).

2.1 Basic equations

As previously noted, secondaries produced by shock accelerated CRp have the wrong spatial profile to explain RH observations. Because they arise from a two body process, they are too centrally concentrated. They also produce gamma-ray emission in excess of Fermi-LAT upper limits (Arlen et al. 2012; Brunetti et al. 2012; Ackermann et al. 2014; Ahnen et al. 2016).

Given a seed population of CRs, we adopt essentially the same set of plasma physics assumptions as the reacceleration model for RHs (Brunetti & Lazarian 2007, 2011). We solve the isotropic, gyro-phase averaged Fokker-Planck equation (via a Crank-Nicholson scheme) for the time evolution of the CRe distribution in the Lagrangian frame (Brunetti & Lazarian 2007, 2011):

$$\begin{aligned} \frac{df_e(p, t)}{dt} &= \frac{\partial}{\partial p} \left\{ f_e(p, t) \left[\left. \frac{dp}{dt} \right|_{\text{Coul}} + \frac{p}{3} (\nabla \cdot \mathbf{v}) + \left. \frac{dp}{dt} \right|_{\text{rad}} \right. \right. \\ &\quad \left. \left. - \frac{1}{p^2} \frac{\partial}{\partial p} (p^2 D_{pp}) \right] \right\} - (\nabla \cdot \mathbf{v}) f_e(p, t) \\ &\quad + \frac{\partial^2}{\partial p^2} [D_{pp} f_e(p, t)] + Q_e [p, t; f_p(p, t)]. \end{aligned} \quad (1)$$

Here f_e is the one-dimensional distribution in position x (suppressed for clarity), momentum $p = P/(m_e c)$ and time t (which is normalised such that the number density is given by $n_{\text{CRe}}(t) = \int dp f_e(p, t)$), $d/dt = \partial/\partial t + \mathbf{v} \cdot \nabla$ is the Lagrangian derivative, \mathbf{v} is the gas velocity, $|dp/dt|$ represents Coulomb (Coul, Gould 1972) and radiative (rad, Rybicki & Lightman

1979) losses, respectively,

$$\begin{aligned} \left. \frac{dp}{dt} \right|_{\text{Coul}} &= \frac{3 \sigma_T n_e c}{2 \beta_e^2} \left[\ln \left(\frac{m_e c^2 \beta_e \sqrt{\gamma - 1}}{\hbar \omega_{\text{plasma}}} \right) \right. \\ &\quad \left. - \ln(2) \left(\frac{\beta_e^2}{2} + \frac{1}{\gamma} \right) + \frac{1}{2} + \left(\frac{\gamma - 1}{4\gamma} \right)^2 \right], \end{aligned} \quad (2)$$

$$\left. \frac{dp}{dt} \right|_{\text{rad}} = \frac{4}{3} \frac{\sigma_T}{m_e c} \frac{p^2}{\beta_e} \left[1 + \left(\frac{B}{B_{\text{CMB}}} \right)^2 \right] \varepsilon_{\text{CMB}}. \quad (3)$$

Here $\beta_e = p/\sqrt{1+p^2}$ is the dimensionless velocity of CRs, $\gamma = \sqrt{1+p^2}$ is the Lorentz factor of CRs, $\omega_{\text{plasma}} = \sqrt{4\pi e^2 n_e/m_e}$ is the plasma frequency, n_e is the number density of free electrons, and $\sigma_T = 8\pi e^4/3(m_e c^2)^2$ is the Thomson cross section. The *rms* magnetic field strength is denoted by B and the equivalent field strength of the cosmic-microwave background is given by $B_{\text{CMB}} = 3.24(1+z)^2 \mu\text{G}$, where z denotes the redshift. In the peripheral cluster regions, where $B \ll B_{\text{CMB}}$, the CRs lose virtually all their energy by means of inverse Compton emission. D_{pp} is the momentum space diffusion coefficient (see Section 2.2), and Q_e denotes the injection rate of primary and secondary electrons in the ICM (see section 3.1). The first term containing the expression $\nabla \cdot \mathbf{v}$ represents Fermi-I acceleration and the second term of this form describes adiabatic gains and losses.

During post-processing of our Coma-like cluster simulation, we solve the Fokker-Planck equation over a redshift interval from $z = 5$ to 0. The simulated cluster undergoes a major merger over the last 1-2 Gyrs that is thought to inject large turbulent eddies. As is commonly assumed (Brunetti & Lazarian 2007, 2011; Yan & Lazarian 2004; Beresnyak et al. 2013) we assume that about one Gyr after core passage the fields have decayed down to the smallest scales k_{cut} , and the radio halo turns on shortly after. We choose this simulation snapshot to analyse. Note that in recent simulations by Miniati (2015), the turbulent reacceleration is strongest around core passage. However, we are not very sensitive to the adopted decay time, since the thermal and CR quantities are very similar a few 100 Myrs before and after $z = 0$, where we have chosen to evaluate the simulations. In all our calculations we assume that turbulent reacceleration efficiently accelerates particles for $\tau_{\text{cl}} \sim 650$ Myrs (which is roughly the cascade time on which turbulence is damped) and that during this turbulent phase CR streaming and spatial diffusion can be neglected. In Section 4.3, we explore sensitivity to the last assumption.

Thus far, we have ignored CR transport. However, if CRs stream in the ICM, then their spatial profile could potentially flatten sufficiently (Enflin et al. 2011; Wiener et al. 2013). This scenario is very attractive: it generates seed electrons with the right spatial footprint, and by removing CRps from the core, obeys gamma-ray constraints. Turbulence plays two opposing roles: Alfvénic turbulence damps waves generated by the CR streaming instability (Yan & Lazarian 2002; Farmer & Goldreich 2004), thus reducing self-confinement; but compressible fast modes scatter CRs directly. Turbulent damping is still efficient for highly subsonic conditions (Wiener et al. 2013), while we assume compressible fast modes to only provide effective spatial confinement during the periods of transsonic, highly super-Alfvénic ($\mathcal{M}_A \sim 5$) turbulence associated with mergers. Thus, CRs can stream out when the cluster is kine-

matically quiescent. Furthermore, even Alfvénic streaming timescales are relatively short (~ 0.1 – 0.5 Gyr; Wiener et al. 2013) compared to the timescale on which the CRp population is built up. Based on these findings, we adopt a toy model for our *M-streaming* scenario in which CR streaming instantaneously produces flat CRp profiles. We assume that CRs cannot stream significantly past perpendicular \mathbf{B} -fields at the accretion shock, so that the total number of CRs is conserved within the virial radius during the streaming process.

The time evolution of the spectral energy distribution of CRps, f_p , is similarly given by:

$$\begin{aligned} \frac{df_p(p, t)}{dt} = & \frac{\partial}{\partial p} \left\{ f_p(p, t) \left[\left. \frac{dp}{dt} \right|_{\text{Coul}} + \frac{p}{3} \nabla \cdot (\mathbf{v} + \mathbf{v}_{\text{st}}) \right. \right. \\ & \left. \left. - \frac{1}{p^2} \frac{\partial}{\partial p} (p^2 D_{pp}) \right] \right\} - f_p(p, t) \nabla \cdot (\mathbf{v} + \mathbf{v}_{\text{st}}) - \mathbf{v}_{\text{st}} \cdot \nabla f_p(p, t) \\ & + \frac{\partial^2}{\partial p^2} [D_{pp} f_p(p, t)] - \frac{f_p(p, t)}{\tau_{\text{had}}(p)} + Q_p(p, t), \end{aligned} \quad (4)$$

where $\mathbf{v}_{\text{st}} = -v_A \nabla f_p / |\nabla f_p|$ is the streaming velocity in the isotropic transport approximation, v_A is the Alfvén speed, and $Q_p(p, t)$ denotes the injection rate of shock accelerated CRps as a function of momentum $p = P/(m_p c)$ and time t (see section 3.1). The timescale of hadronic losses that produce pions via CRp collisions with thermal protons of the ICM is given by

$$\tau_{\text{had}} = [c n_{\text{th}} \sigma^{+/-0}(p)]^{-1}, \quad (5)$$

where we use the cross-section, $\sigma^{+/-0}(p)$, given by the fitting formula in Dermer (1986).

2.2 Turbulent reacceleration

In turbulent reacceleration, particles gain energy via Fermi II acceleration. Wave-particle energy exchange takes place via transit time damping (TTD, Brunetti & Lazarian 2007, 2011). The TTD resonance requires the wave frequency to obey the resonance condition, $\omega = k_{\parallel} v_{\parallel}$, where k_{\parallel} and v_{\parallel} are the parallel (projected along the magnetic field) wavenumber of the compressible mode and particle velocity, respectively. This implies that the particle transit time across the confining wave region matches the wave period, $\lambda_{\parallel}/v_{\parallel} = \tau_{\text{wave}}$ (hence the moniker, ‘transit time damping’). Note that the CRs’ gyroradius does not enter the resonance condition. Hence the CRs that are in resonance with compressible waves experience Fermi-II acceleration irrespective of the length scale of the perturbation.

However, the resonance changes the component of the particle momentum parallel to the mean magnetic field, which over time leads to increasing anisotropy in the particle distribution that decreases the efficiency of reacceleration with time. As in Brunetti & Lazarian (2011), we assume that there exists a mechanism—such as the firehose instability—that isotropises the CR distribution function at the gyroscale and on the reacceleration time scale, which ensures sustained efficient reacceleration with time.

All of the physics of turbulent reacceleration is effectively encapsulated in the diffusion coefficient (Brunetti & Lazarian 2007), which can be rewritten as

(Miniati 2015):

$$D_{pp}(p) = \frac{p^2 \pi I_{\theta}(c_s/c)}{8c} \langle k \rangle_{\mathcal{W}} \langle (\delta v_c)^2 \rangle \quad (6)$$

where I_{θ} averages interaction rates over the CR pitch angle θ ; $I_{\theta} \approx 5$ for ICM conditions, and

$$\langle k \rangle_{\mathcal{W}} = \frac{1}{\langle (\delta v_c)^2 \rangle} \int_{k_L}^{k_{\text{cut}}} dk k \mathcal{W}(k) \approx \frac{s-1}{2-s} k_L \left(\frac{k_{\text{cut}}}{k_L} \right)^{2-s} \quad (7)$$

is an energy-averaged wavenumber, k_L, k_{cut} are the wavenumbers associated with the outer scale L and the cutoff scale respectively, and we have assumed a total energy spectrum (composed of both kinetic and potential energy, where the two are assumed to be in equipartition, Sarkar et al. 1991):

$$\mathcal{W}(k) = \frac{(s-1) \langle (\delta v_c)^2 \rangle}{k_L} \left(\frac{k}{k_L} \right)^{-s} \quad (8)$$

which defines the normalisation $\langle (\delta v_c)^2 \rangle$ (the subscript ‘c’ emphasizes that we specialise to compressive modes). Intuitively, we can understand the form of the diffusion coefficient from the fact that for second-order Fermi acceleration, $\dot{p} \sim \Delta p / \tau \sim p \langle kc \rangle_{\mathcal{W}} (\delta v_c / c)^2$, where $\tau^{-1} \sim \langle kc \rangle_{\mathcal{W}}$ is the energy averaged wave-particle interaction rate, and $\Delta p \sim p (\delta v_c / c)^2$ is the typical momentum change during wave-particle scattering. Thus:

$$D_{pp} \sim p \dot{p} \sim p^2 \langle kc \rangle_{\mathcal{W}} \left(\frac{\delta v_c}{c} \right)^2. \quad (9)$$

Equations (6) and (8) make the important aspects of turbulence clear: the energy in compressive modes $\langle (\delta v_c)^2 \rangle$, the inner and outer scale (k_{cut} and k_L), and the slope of the energy spectrum s . All of these can vary spatially and temporally.

We adopt a Kraichnan spectrum ($s = 3/2$) for the fast modes, as seen in simulations (Cho & Lazarian 2003). This can also be written as:

$$\mathcal{W}(k) = \sqrt{2/7} I_L \rho \langle v_{\text{ph}} \rangle k^{-3/2}, \quad (10)$$

where I_L is the volumetric injection rate of turbulence at scale L (which is assumed to be constant), $v_{\text{ph}} \approx c_s$ is the phase speed of waves. Since the Kraichnan spectrum is critical in what follows, it is worthwhile taking a moment to recount the origin of the spectral slope s and the cascade rate. In the magnetically dominated regime, two counter-propagating wave packets of scale l interact on a wave crossing time $\tau_{\text{ph}} = l/v_{\text{ph}}$, rather than the eddy turnover time $\tau_{\text{edd}} = l/v_l$. Since $\tau_{\text{ph}} \ll \tau_{\text{edd}}$, each interaction results in a small velocity change $\delta v_l \sim v_l (\tau_{\text{ph}} / \tau_{\text{edd}})$. If these changes behave like a random walk, the cascade time τ_1 it takes for an eddy to become non-linear ($\Delta v \sim v_l$) and cascades to smaller scales occurs with a characteristic velocity $v_1 \sim \delta v_l (\tau_1 / \tau_{\text{ph}})^{1/2} \sim v_l (\tau_{\text{ph}} / \tau_{\text{edd}}) (\tau_1 / \tau_{\text{ph}})^{1/2}$, which we can solve to obtain the cascade time:

$$\tau_1 \sim \left(\frac{\tau_{\text{edd}}}{\tau_{\text{ph}}} \right)^2 \tau_{\text{ph}} \sim \frac{l v_{\text{ph}}}{v_l^2} \quad (11)$$

where we have implicitly assumed isotropy. This implies a dissipation rate $\epsilon \sim v_l^2 / \tau_1 \sim v_l^4 / (l v_{\text{ph}})$, or $v_l \sim (\epsilon l v_{\text{ph}})^{1/4}$. Thus, since $kE(k) \sim v_l^2$, this gives a kinetic energy spectrum:

$$E(k) \sim (\epsilon v_{\text{ph}})^{1/2} k^{-3/2}. \quad (12)$$

It is important to realise that this Kraichnan scaling

only applies at small scales, where turbulence is magneto-hydrodynamical. At large scales, turbulent motions are subsonic ($\mathcal{M}_s \sim 0.2 - 0.5$) but super-Alfvénic ($\mathcal{M}_A \sim 5$). Thus, except in the case where motions are transsonic and weak shocks become important, motions are fundamentally hydrodynamic and turbulence follows a Kolmogorov ($s = 5/3$) spectrum. However, while the turbulent energy density $\varepsilon_{\text{turb}} \propto l^{2/3}$ decreases at small scales, the magnetic energy density (which is dominated by the large scale mean field) is scale-independent. Thus, at some scale $l_A \sim l_L \mathcal{M}_A^{-3}$, where $\varepsilon_{\text{turb}} \sim \varepsilon_B$, the magnetic field becomes dynamically important, and turbulence transitions to the MHD regime. The cutoff scale in equation (8) can be computed by setting the turbulent cascade rate for fast modes to the transit time damping rate on thermal electrons. This yields (Brunetti & Lazarian 2007; Miniati 2015):

$$k_{\text{cut}} \approx Ak_{\text{outer}} \frac{((\delta v_{\text{outer}})^2)^2}{c_s^4} \quad (13)$$

where $A \approx 11000$. If there is an unimpeded cascade from the injection to the cutoff scale, $k_{\text{outer}} = k_L$ and $v_{\text{outer}} = v_c$. However, in our case the hydrodynamic (Kolmogorov) cascade transitions to the MHD cascade at the Alfvén scale so that $k_{\text{outer}} = k_A$ and $v_{\text{outer}} = v_A$ and hence, we get¹

$$k_{\text{cut}} \approx Ak_A \beta^{-2}. \quad (14)$$

This gives $2\pi/k_{\text{cut}} \sim 0.1 - 1$ kpc in the ICM. This constitutes an effective mean free path for CRs, unless plasma instabilities can mediate interactions between turbulence and particles on smaller scales (Brunetti & Lazarian 2011), a possibility we discuss in Section 4.3. Another possibility is that compressible modes dissipate in weak shocks, resulting in Burgers' turbulence $s = 2$ (Kowal & Lazarian 2010; Porter et al. 2015; Miniati 2015). If Burgers turbulence dominates, then particle acceleration rates are too slow in the face of cooling processes to explain radio haloes (Miniati 2015), and an alternative model for radio haloes is required.

The spatial profile of injected turbulence depends on the details of the merger such as time during the merger, the impact parameter, the merger mass ratio, and the degree of cluster anisotropy (Miniati 2015). We parametrize these uncertainties and assume that volumetric injection rate of turbulent energy, $I_L \propto \varepsilon_{\text{th}}^{\alpha_{\text{tu}}}$, and determine the normalisation by requiring that the turbulent energy in compressible modes $E_{\text{turb}} = \int \int \mathcal{W}(k) dk dV = X_{\text{tu}} E_{\text{th}}$, where E_{th} is the total thermal energy. Given these definitions, one can show that:

$$D_{pp} \propto \frac{I_L}{\rho c_s} \propto X_{\text{tu}}^2 k_L \varepsilon_{\text{th}}^{\alpha_{\text{tu}}-1} \sqrt{T}. \quad (15)$$

What is a typical energy density in compressive fast modes? The total turbulent energy is typically $\sim 15 - 70$ per cent of the thermal energy in a cluster (Vazza et al. 2011a); it rises rapidly during a merger. The compressible component is $\sim 20 - 40$ per cent of the total turbulent energy, and shows more rapid temporal variations compared to the incompressible component (Beresnyak et al. 2013; Miniati

2015). Note the compressible component in cluster simulations is much larger than in stirring box simulations with similar Mach numbers (Kowal & Lazarian 2010; Lynn et al. 2014). This is likely due to the compressive nature of turbulent driving (transsonic infall and merger), whereas idealised simulations tend to use incompressible solenoidal driving and allow compressive fluctuations to develop on their own. Overall, we adopt a compressive energy density which is $X_{\text{tu}} \sim 0.2$ of the thermal energy as a baseline estimate.

The important effects are best summarised in terms of the acceleration rate which is governed by advection in momentum space:

$$\tau_{\text{D}}^{-1} \equiv \Gamma_{\text{D}} \equiv \frac{\dot{p}}{p} = p^{-3} \frac{\partial}{\partial p} (p^2 D_{pp}) = \frac{4D_{pp}}{p^2}. \quad (16)$$

In the last step we have used that $D_{pp} \propto p^2$ for turbulent reacceleration (equation 9). Hence the acceleration time is independent of momentum. This should be compared against the lifetime of turbulence, τ_{cl} , and the cooling time τ_{cool} . In Table 1, we show both the thermal quantities and the timescales for CR cooling and (re)acceleration for three different spatial regions of the RH. The densities (Briel et al. 1992) and temperatures (Bonamente et al. 2009; Arnaud et al. 2001) are derived from X-ray observations. To calculate synchrotron cooling times, we use B -fields derived from Faraday rotation measurements (Bonafede et al. 2010). To calculate the acceleration time, we need to assume an outer scale. We assume an injection scale $k_L = 2\pi/\lambda_L$, where $\lambda_L = 100$ kpc, which were assumptions adopted in previous work (Subramanian et al. 2006; Brunetti & Lazarian 2007, 2011). This length scale corresponds to an eddy turnover time on the outer scale of $2\pi\lambda_L v_L^{-1} \sim 1.2$ Gyr if $v_L \sim 500 \text{ km s}^{-1}$, as is characteristic of a merger. Note that hydrodynamical simulations of clusters have sometimes found larger λ_L , in some cases comparable to the size of the cluster (e.g. $\lambda_L \sim 1 \text{ Mpc}$ in Vazza et al. 2011a; Miniati 2015). This choice is degenerate with X_{tu} ; in Section 4.3 we argue that k_A is a more appropriate choice, but also find that when the decay time is appropriately scaled, we are relatively insensitive to the choice of k_L . We present τ_{D} for 3 different models, which we discuss in the next section. The reacceleration timescale τ_{D} is similar between our three models, where the difference comes from turbulent profile parametrized with α_{tu} . This implies that even small differences in the turbulent profile could impact the seed CRs significantly. Finally, we adopt an duration of acceleration $\tau_{\text{cl}} = 650$ Myr, in line with previous assumptions (Brunetti & Lazarian 2007), roughly corresponding to the turbulent decay time.

3 COSMOLOGICAL SIMULATIONS

In this section, we solve the Fokker-Planck equation for CR transport on Lagrangian particle trajectories through cosmic history. We then use our parametrized model of turbulence to apply turbulent re-acceleration, and compare radio halo profiles against observations of the Coma cluster. We follow the philosophy of adopting assumptions roughly in line with previous successful models, which are now confronted with more accurate calculations of the seed CR population, and

¹ Note that this differs from previous work, which assumes Kraichnan turbulence from the injection scale onward and effectively adopts wave number and compressible velocity at the outer scale L for this estimate of k_{cut} .

Table 1. Thermal quantities and timescales for different spatial regions in a Coma like cluster.

	spatial regions		
	$0.1 R_{\text{RH}}^{(2)}$	$0.3 R_{\text{RH}}^{(2)}$	$R_{\text{RH}}^{(2)}$
thermal quantities ⁽¹⁾			
ρ [10^{-27} g cm ⁻³]	3.0	1.6	0.15
T [10^8 K]	1.4	1.0	0.58
timescales ⁽¹⁾			
$\tau_{\text{D}}(M\text{-primaries})^{(3)}$ [Gyr]	0.45	0.44	0.39
$\tau_{\text{D}}(M\text{-streaming})^{(3)}$ [Gyr]	0.50	0.47	0.34
$\tau_{\text{D}}(M\text{-turbulence})^{(3)}$ [Gyr]	0.69	0.56	0.27
$\tau_{\text{C/sync}}(P = 10^4 m_e c)^{(4)}$ [Gyr]	0.11	0.15	0.22
$\tau_{\text{had}}(P = 100 m_p c)^{(5)}$ [Gyr]	2.4	4.5	47
$\tau_{\text{Coul}}(P = m_e c)^{(6)}$ [Gyr]	0.0092	0.017	0.17

Notes:

- (1) Median quantities from our simulated post-merging cluster g72a derived during last 300 Myrs in time.
(2) Radius of the giant radio halo in Coma where $R_{\text{RH}} \approx 0.6 R_{200}$.
(3) Fermi-II reacceleration for both electrons and protons at all energies.
(4) Inverse Compton and synchrotron cooling for electrons.
(5) Catastrophic losses for protons.
(6) Coulomb cooling for electrons (protons factor m_e/m_p smaller).

find the minimal modifications required to fit observations. We re-examine these choices in Section 4.

Since the standard vanilla model requires a CR seed population which is inconsistent with the simulations (Figure 1), some modifications are necessary, either in the seed CR population or in the properties of the turbulence. We focus on three scenarios. (i) In model *M-primaries*, we assume that CR electrons, which have been accelerated by cosmic formation shocks and successively cooled by inverse Compton and synchrotron losses, form a fossil seed population for reacceleration. (ii) In model *M-streaming*, we account for the outward streaming of central CRps, which produces a flat CR distribution in the ICM and equivalently a flat secondary seed population of CRes for reacceleration. (iii) In model *M-turbulence* we adopt a spatially flatter turbulent profile than what was adopted before but assume that seed CRps and secondary CRes follow the steep profile that is suggested by structure formation simulations.

3.1 Modelling diffusive shock acceleration

In this paper we focus on our simulated cluster, g72a, which is a massive cluster of mass $M_{200} = 1.6 \times 10^{15} M_{\odot}$ that experienced a merger about 1 Gyr ago (Dolag et al. 2009). Since the cluster mass, density and temperature profiles are all similar to the well studied Coma cluster (Pfrommer et al. 2007; Pinzke & Pfrommer 2010), we will compare our calculations to radio and gamma-ray observations of Coma.

We use a simple test-particle model for the CR acceleration and injection, where each shock injects CRs that trace a power-law in momentum,

$$f_p(p, t) = C(t) p^{\alpha_{\text{inj}}}, \quad \alpha_{\text{inj}} = \frac{(\gamma_{\text{ad}} + 1) \mathcal{M}^2}{(\gamma_{\text{ad}} - 1) \mathcal{M}^2 + 2} \quad (17)$$

determined by the normalisation $C(t)$ and the spectral index

α_{inj} that depends on the adiabatic index $\gamma_{\text{ad}} = 5/3$ and the Mach number of the shock \mathcal{M} (see also Quilis et al. 1998; Miniati et al. 2001a; Pfrommer et al. 2006). It is given by the ratio of the upstream velocity (v_2) and the sound speed (c_s). The CR number density and CR energy density are derived from

$$n_{\text{CR}} = \int_{p_{\text{inj}}}^{\infty} dp f_p(p) \quad (18)$$

$$\mathcal{E}_{\text{CR}} = \int_{p_{\text{inj}}}^{\infty} dp f_p(p) E(p), \quad (19)$$

where $E(p) = (\sqrt{1 + p^2} - 1) m_p c^2$ is the kinetic energy of a proton with momentum p . We adopt a fit to Monte Carlo simulations of the thermal leakage process that relates the momentum of injected protons (p_{inj}) to the thermal energy (p_{th}) of the shocked plasma (Kang & Ryu 2011):

$$p_{\text{inj}} = x_{\text{inj}} p_{\text{th}} = x_{\text{inj}} \sqrt{\frac{2 k_B T_2}{m_p c^2}},$$

$$\text{where } x_{\text{inj}} \approx 1.17 \frac{v_2}{p_{\text{th}} c} \left(1 + \frac{1.07}{\epsilon_B}\right) \left(\frac{\mathcal{M}}{3}\right)^{0.1}. \quad (20)$$

Here $\epsilon_B = B_0/B_{\perp}$, B_0 is the amplitude of the downstream MHD wave turbulence, and B_{\perp} is the magnetic field along the shock normal. The physical range of ϵ_B is quite uncertain due to complex plasma interactions. In this paper, we adopt $\epsilon_B = 0.23$, which – as we will later see – corresponds to a conservative maximum energy acceleration efficiency for protons of 0.1. To derive the acceleration efficiency, ζ_{inj} , we first have to infer the particle injection efficiency, which is the fraction of downstream thermal gas particles which experience diffusive shock acceleration (for details see Pinzke et al. 2013),

$$\eta_{\text{p,lin}} = \frac{4}{\sqrt{\pi}} \frac{x_{\text{inj}}^3}{\alpha_{\text{inj}} - 1} e^{-x_{\text{inj}}^2}. \quad (21)$$

The particle injection efficiency is a strong function of x_{inj} that depends on both \mathcal{M} and ϵ_B . The energy density of CRs that are injected and accelerated at the shock (neglecting the CR back reaction on the shock) is given by

$$\Delta \mathcal{E}_{\text{CR,lin}} = \eta_{\text{p,lin}}(\mathcal{M}) n_{\text{th}}(T_2) \frac{\mathcal{E}_{\text{CR}}}{n_{\text{CR}}} \quad (22)$$

and the CR energy injection and acceleration efficiency is:

$$\zeta_{\text{lin}} = \frac{\Delta \mathcal{E}_{\text{CR,lin}}}{\Delta \mathcal{E}_{\text{diss}}}, \quad \text{where } \Delta \mathcal{E}_{\text{diss}} = \epsilon_{\text{th2}} - \epsilon_{\text{th0}} \left(\frac{\rho_2}{\rho_0}\right)^{\gamma_{\text{ad}}}. \quad (23)$$

The dissipated energy density in the downstream regime, $\Delta \mathcal{E}_{\text{diss}}$, is given by the difference of the thermal energy densities in the pre- and post-shock regimes, corrected for the adiabatic energy increase due to gas compression.

We limit the acceleration efficiency to ζ_{max} by steepening the spectral index of the injected population α_{inj} to α_{sub} so that $\zeta_{\text{lin}} \leq \zeta_{\text{max}}$ is always fulfilled. The slope α_{inj} impact ζ_{lin} via the mean energy per particle, ϵ_p/n_p . This procedure conserves energy and is motivated by models of non-linear shock acceleration where a sub-shock with a lower compression ratio (and hence steeper spectral index) forms (e.g., Ellison et al. 2000). Given our assumed $\epsilon_B = 0.23$, we find that for strong shocks where $\alpha_{\text{inj}} \lesssim 2.3$ the spectral slope is steepened by a maximum of ~ 10 per cent in low temperature regimes ($k_B T \sim 0.1$ keV), while the steepening is much

smaller for high temperature regimes ($k_B T \sim 10$ keV) that are more relevant for clusters. Since p_{inj} remains fixed, so does the CR number density n_{CR} . Hence we can solve for the renormalised normalisation constant C_{sub} using n_{CR} and Eqn. 21:

$$C_{\text{sub}} = \eta_{\text{p,lin}} (\alpha_{\text{sub}} - 1) p_{\text{inj}}^{\alpha_{\text{sub}} - 1}, \quad (24)$$

where the new distribution function is given by $f_p(p, t) = C_{\text{sub}} p^{-\alpha_{\text{sub}}}$. We set an upper limit on the ratio of accelerated proton-to-dissipated energy in the downstream of strong shocks that varies from $\zeta_{\text{max}} \sim 0.01 - 0.1$, depending on the adopted model (for more details, see section 3).

In our Galaxy, the CRe-to-CRp ratio at a few GeV is $K_{\text{ep}} \approx 10^{-2}$. Hence, we adopt this as a fiducial value for the CRe-to-CRp acceleration efficiency in our models *M-streaming* and *M-turbulence* (see Pinzke et al. 2013, for more discussion). However, as recent PIC simulations have shown, this is likely very different at weak shocks, with electrons efficiently accelerated at perpendicular shocks (Guo et al. 2014a,b), and ions (and electrons) efficiently accelerated at parallel shocks (Caprioli & Spitkovsky 2014; Park et al. 2015). Thus, depending on magnetic geometry, K_{ep} could be either larger or smaller. Some observations of radio relics suggest high values of K_{ep} , due to the absence of gamma-ray emission, which probes the CRp population (Vazza & Brügggen 2014). This suggests primary CRes as a viable alternative scenario to secondary CRes as seeds for the giant RHs. In our *M-primaries* scenario, the injected distribution of CRes is derived in the same way as for the CRps. Once they have been accelerated to relativistic energies, injected electrons and protons are indistinguishable. We therefore assume that CRp and CRe have the same distribution function $f_e(p) = K_{\text{ep}} f_p(p)$, with a different normalisation (due to differing acceleration efficiencies) $K_{\text{ep}} = 0.1$ (which is viable for primarily perpendicular shocks, Guo et al. 2014a). Given the unknown magnetic geometry at cluster shocks, we investigate the consequences of this additional degree of freedom.

3.2 Radio emission profile

In Figure 2, we show radial profiles for the radio emission in all three scenarios in which the seeds undergo Fermi-II reacceleration in turbulent fields that are shaped such as to reproduce the Coma RH profile at 352 MHz. Adopting our parametrization for the volumetric injection rate of turbulent energy, $I_L \propto \varepsilon_{\text{th}}^{\alpha_{\text{tu}}}$, we find that to fit the observations, we require $\alpha_{\text{tu}} = 0.67$ for *M-turbulence*, $\alpha_{\text{tu}} = 0.82$ for *M-streaming*, and $\alpha_{\text{tu}} = 0.88$ for *M-primaries*. As a result, the ratio of turbulent-to-thermal energy densities slightly increase with radius as shown in Figure 3. The fine-tuning of these exponents is somewhat problematic, as we discuss in Section 4. After turbulent reacceleration, the volume-weighted, relative CRp energy density and relative CRp number density inside the RH for *M-turbulence* (*M-streaming*), are found to be 2 (3) per cent and 2×10^{-8} (5×10^{-8}), respectively.

Figure 2 demonstrates that the modelled radio profiles without turbulent reacceleration are too steep. In the bottom right panel of Figure 2 (labelled with Brunetti et al. 2012), we show that our simulated profiles of reaccelerated CRs, which only take advective CR transport into account,

i.e. they neglect CR streaming or a flatter turbulent profile, produce radio profiles that are too steep. Indeed, even using the assumptions of previous work, where complete freedom in the seed population was allowed, it is not possible to reproduce observations in both frequencies in any model² – with or without turbulent reacceleration. Decreasing the acceleration efficiency with radius does not change this conclusion much because of the weak radial dependence of $D_{pp}(R) \propto \varepsilon_{\text{th}}(R)^{\alpha_{\text{tu}} - 1} \sqrt{T(R)}$. This signals that the problem is generic and requires either additional modifications to the plasma physics of acceleration or a better understanding of potential observational systematics. In addition there are differences in the simulated density and temperature profiles in comparison to the observed profile in Coma that impact the CR abundance as well as cooling and reacceleration.

In Figure 4 we show how the turbulent reacceleration timescales in our three models scale with radius. As expected, the *M-primaries* model with $\alpha_{\text{tu}} = 0.88$ has the flattest profile with $\tau_D \approx 0.4$ Gyr, where the small dip at large radius driven by the decrease in thermal energy density. The *M-turbulence* model has the flattest turbulent profile parametrized by the smaller α_{tu} which explains the steepest τ_D profile. Note that a fixed reacceleration timescale is required to explain the observations at each radius and for each model (see also Table 1). Since $\tau_{\text{cl}} \propto X_{\text{tu}}^2 k_L$, these two parameters are degenerate and can be traded off one another.

In principle, reacceleration via TTD leads to spectral steepening with particle energy due to the inefficiency of the acceleration process to counter the stronger cooling losses with increasing energy. Since synchrotron emission peaks at frequency $\nu_{\text{syn}} \approx 1 B/\mu\text{G}(\gamma/10^4)^2$ GHz, this translates into a spectral steepening of the radio spectrum (see the left panel of Figure 5 where the continuous injection of secondary CRes is absent). A given radio window samples higher energy electrons for a decreasing field strength in the cluster outskirts. Hence, the spectral steepening with energy should translate into a radial spectral steepening (Brunetti et al. 2012). However, because of the weak dependence of the electron Lorentz factor on emission frequency ($\gamma \propto \sqrt{\nu_{\text{syn}}}$), this effect is only visible in our simulations for $\nu_{\text{syn}} \gtrsim 5$ GHz. Most importantly, our simulated fluid elements at a given radius sample a broad distribution of shock history, density and temperature, which implies very similar synchrotron brightness profiles at $\nu_{\text{syn}} = 352$ MHz and 1.4 GHz. The discrepancy of the observed and simulated 1.4 GHz profiles could instead be due to systematic flux calibration error in single dish observations. These could arise, for instance, due to errors in point source subtraction. Interestingly, we can match the 1.4 GHz data if we reduce the zero point by adding 0.1 of the central flux to every data point; this flattens the outer profile³. Alternatively, this may point to weaknesses in the theoretical modelling of the particle acceleration process and may require a stronger cutoff in the particle energy spectrum.

² Note that in previous work on the Coma cluster, $\varepsilon_{\text{turb}} \propto \varepsilon_{\text{th}}$ was adopted which approximately corresponds to $\alpha_{\text{tu}} = 1$ (Brunetti et al. 2012) and together with the different distributions for seed CRes constitute the main differences compared to our work.

³ Lawrence Rudnick, private communication.

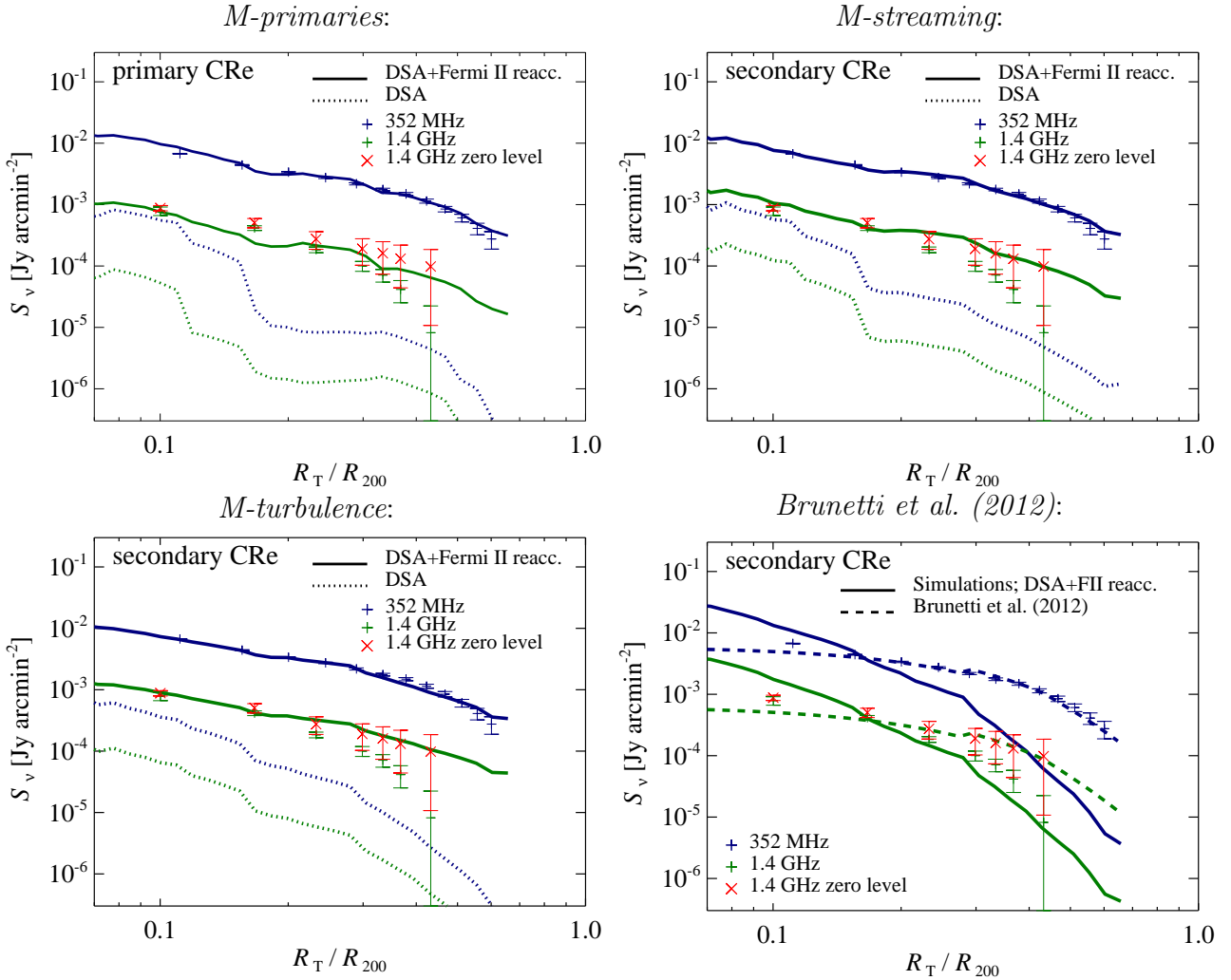


Figure 2. Radio surface brightness profiles of Fermi-II reaccelerated CR electrons of a simulated post-merging cluster similar to Coma. We compare profiles at 352 MHz (blue lines and crosses, [Brown & Rudnick 2011](#)) to those at 1.4 GHz (green lines and crosses, [Deiss et al. 1997](#)). The red crosses show the reprocessed 1.4 GHz data, where a zero level of about 0.1 of the central value is adopted. The solid lines show predicted emission from a reaccelerated fossil population, while dotted lines show emission from a fossil population without reacceleration. The panels show the emission of our models *M-primaries* (upper left panel), *M-streaming* (upper right panel), *M-turbulence* (lower left panel), and simulated secondary electrons together with previous estimates ([Brunetti et al. 2012](#)) for the Coma cluster (lower right panel).

3.3 Radio spectrum

In Figure 5 we show that our three models that include Fermi-II reacceleration can individually reproduce the convexly curved total radio spectrum found in the Coma cluster. Seed CRs in *M-streaming* and *M-turbulence* that do not experience turbulent reacceleration have a power-law spectrum in disagreement with observations. In order to match both the spatial and spectral profiles in Coma, we adopt an acceleration efficiency for the strongest shocks in our three models *M-primaries*, *M-streaming*, and *M-turbulence* to $\zeta_e < 0.003$, $\zeta_p < 0.1$, and $\zeta_p < 0.03$, respectively. Following the Mach number (\mathcal{M})-dependence of the acceleration efficiency suggested in [Pinzke et al. \(2013\)](#), the efficiency in weak shocks ($\mathcal{M} \sim 2.5\text{--}3.5$) that dominates the CR distribution function, has an acceleration efficiency for protons $\zeta_p \sim 0.0001\text{--}0.01$, and for electrons $\zeta_e \sim 0.001$.

Interestingly, we find that the radio luminosity from

clusters in the OFF-state (DSA only) and ON-state (DSA and reacceleration) differ by about a factor 10-20 in all our three models. This means that the secondary CREs are dominated by the reaccelerated fossil CREs and not from the CREs produced by reaccelerated CRps. However, for high frequencies ($\nu_{\text{syn}} \gtrsim \text{GHz}$) where synchrotron cooling is more efficient than reacceleration, the emission is dominated by the CREs produced in the continuous injection of electrons from reaccelerated CRps. It is also worth mentioning that the radio emission from secondary CREs are smoothly distributed around the cluster because of the continuous injection, hence it is not dominated by outliers.

However, for *M-primaries*, the primary CREs that generate most of the radio emission from the cluster in the OFF-state are dominated by only a small fraction of the CREs. These electrons are injected very recently and have not had time to cool yet. Hence we expect there to be a large variance in the OFF-state of different simulated clusters. As

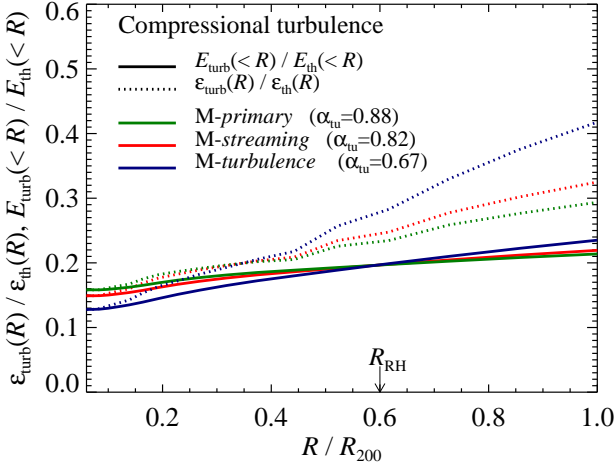


Figure 3. The ratio of turbulent-to-thermal energy densities (solid lines) and cumulative energies (dotted lines) in our three models. The energy densities are parametrized as $\epsilon_{\text{turb}} \propto \epsilon_{\text{th}}^{(\alpha_{\text{u}}+1)/2} T^{-1/4}$ and normalised such that the total turbulent energy in compressible modes E_{turb} for each scenario makes up about 20 per cent of the total thermal energy E_{th} inside the radio halo ($R_{\text{RH}} \approx 0.6R_{200}$). The turbulent profiles explore the uncertainty in the cluster turbulence and are motivated by the cosmological simulation in (Lau et al. 2009; Shaw et al. 2010; Vazza et al. 2011b).

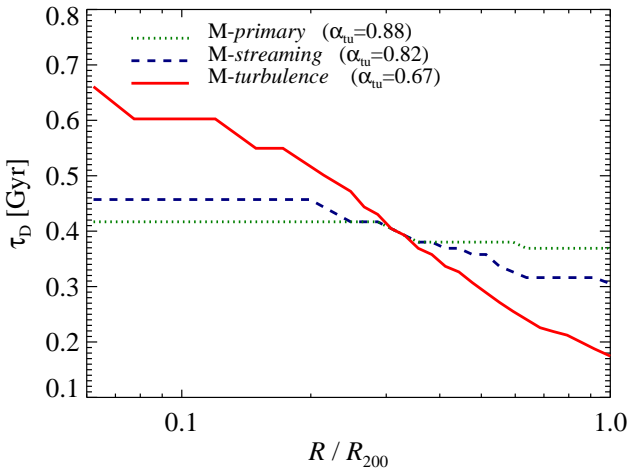


Figure 4. Turbulent reacceleration timescales for our simulated cluster g72a. We show in linear-log the reacceleration timescale (τ_{D}) as a function of radius R for our three models: *M-primaries* (green dotted line), *M-streaming* (blue dashed line), and *M-turbulence* (red solid line). Note that the timescales are derived during the last 100 Myrs in time in our simulations.

mentioned in section 4, combining radio observations with gamma-ray limits allows us to put a lower limit to X_{tu} . If X_{tu} is smaller than in our adopted models (where we assume $X_{\text{tu}} = 0.2$), then the efficiency of DSA has to be larger than $\zeta_{\text{p}} \sim 0.1$ for the secondary CRs to reproduce the radio observations. However, since the turbulent reacceleration acts on both the secondary CRs and the CRps, while ζ_{p} only affects the CRps, *M-streaming* and *M-turbulence* would produce too much gamma-rays. Hence we conclude that $X_{\text{tu}} \gtrsim 0.2$ if all other parameters are kept fixed. Although, we caution the

reader to take this limit too stringent because of the uncertainty in k_L and τ_{cl} that impact X_{tu} for a fixed τ_{D} . This parameter space needs to be explored further in future work in order to put more stringent limits on the level of turbulence in clusters using radio and gamma-ray observations in combination with turbulent reaccelerated CRs.

3.4 Gamma rays

The gamma-ray emission from CRps that produce decaying neutral pions could be substantial if the CRps are reaccelerated efficiently enough, hence it is interesting to estimate this emission for our models and compare to upper limits. We follow the formalism outlined in Blasi & Colafrancesco (1999) (and references therein) and calculate the gamma-ray emission numerically for our three models. We predict the gamma-ray emission from *M-turbulence* (*M-streaming*) with $F_{\gamma}(> 500 \text{ MeV}) = 4 \times 10^{-10} (5 \times 10^{-10}) \text{ ph s}^{-1} \text{ cm}^{-2}$. The fluxes from these models are slightly larger than in Brunetti et al. (2012), where the differences comes from our steeper CRp profiles in addition to the simulation based formalism we rely on that accounts for both Coulomb and hadronic losses during the build up of the CR distribution in contrast to the scaling relations adopted in their paper. Interestingly the gamma-ray flux from both our scenarios are just below recent Fermi-LAT limits derived from a gamma-ray profile similar to *M-turbulence*⁴ where $F_{\gamma}(> 500 \text{ MeV}) < 5.3 \times 10^{-10} \text{ ph s}^{-1} \text{ cm}^{-2}$. The spectral index of the CRp distribution is relatively steep ($\alpha_{\text{p}} \sim 2.6$) for the CRp energies $E \gtrsim 10 \text{ GeV}$ that are relevant for the injection of radio-emitting secondary CRs. The steep spectrum is ultimately a consequence of the shock history of the simulated cluster, with a weak dependence on our test particle model for Fermi-I acceleration (Pinzke et al. 2013), where we steepen the spectral index to avoid acceleration efficiencies above $\zeta_{\text{p}} \sim 0.1$.

4 PARAMETER SPACE EXPLORATION AND OVERCOMING FINE TUNING

In this paper we rely on several critical parameters describing relatively unknown non-thermal physics in the ICM. Here we develop a simplified framework for our reacceleration model of secondary electrons. We will explore how radio emission depends on the parameters describing the spatial profile of CR protons and turbulence. Our fiducial model is meant to be compared against the Coma cluster.

4.1 Methodology

As we have seen before, the most uncertain aspects of radio halo emission models are the profile of compressible turbulence (which determines the amount of Fermi II acceleration) and the distribution of pre-existing CRs. Hence we vary parameters describing the amount of energy contained in turbulence, X_{tu} (defined by $E_{\text{turb}} = X_{\text{tu}} E_{\text{th}}$), the spatial profile

⁴ Fabio Zandanel, private communication; see also Zandanel & Ando (2014); Ackermann et al. (2014); this will be probed in the next few years by Fermi-LAT.

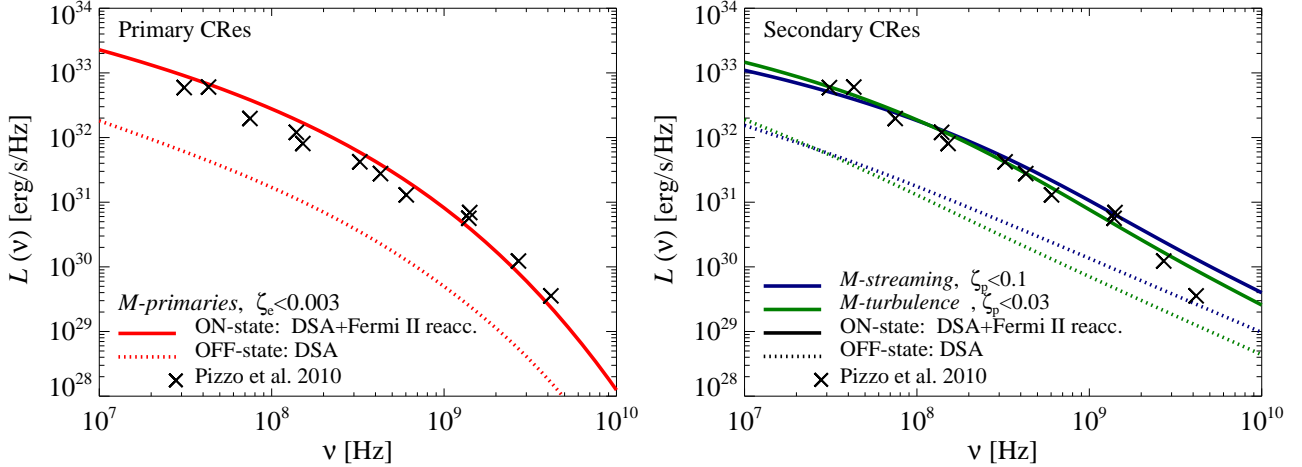


Figure 5. Radio synchrotron spectra. Lines are derived from simulations, while the black crosses are compiled from observations [Pizzo \(2010\)](#). The solid lines show the DSA and reaccelerated CRs (On-state of the radio halo), while the dotted lines show CRs accelerated only by DSA (Off-state of the radio halo). The left figure shows the radio emission induced by primary CRes and the right figure shows the emission from secondary CRes. The different line colours represent our different models, *M-primaries* (red line), *M-streaming* (blue line), and *M-turbulence* (green line).

of turbulence as parametrized by α_{tu} (defined by $I_L \propto \varepsilon_{\text{th}}^{\alpha_{\text{tu}}}$, where $I_L \propto v_L^3 k_L$ is the injection rate of turbulence), as well as the spatial CR profile that we will parametrize by $\alpha_{\text{CR,spat}}$ (see below). We hold fixed thermal plasma properties (temperature and density profiles), B -field profiles, total CR energy content, and the turbulent outer scale (corresponding to a wavenumber k_L). The CR energy content is suggested by our simulations (observations only give an upper bound; [Arlen et al. 2012](#)). We focus on the uncertain CR distribution rather than the overall normalisation, since the impact of the latter (an overall linear scaling) is clear.

In order to quickly explore this parameter space, we solve the Fokker-Planck equation in static spherical shells for injection, reacceleration, and losses of the CRs, i.e., we neglect Lagrangian evolution during re-acceleration. This ignores the effect of adiabatic compressive heating of the CRs, though this is generally subdominant (e.g., see Figure 7 of [Minati 2015](#)). Once the CRs have been reaccelerated for $\tau_{\text{cl}} = 650$ Myr, we calculate the resulting radio emission numerically using the formalism outlined in [Rybicki & Lightman \(1979\)](#) and compare the emission profiles and spectra as we vary one parameter at a time relative to our fiducial model.

We adopt both the density ([Briel et al. 1992](#)) and temperature profiles ([Bonamente et al. 2009](#); [Arnaud et al. 2001](#)) derived from X-ray observations of the Coma cluster,

$$\begin{aligned} n_e &= n_0 \left[1 + (R/R_c)^2 \right]^{-1.125}, \\ k_B T &= 8.25 \text{ keV} \left[1 + (2R/R_{200})^2 \right]^{-0.32}, \end{aligned} \quad (25)$$

with $n_0 = 3.4 \times 10^{-3} \text{ cm}^{-3}$. The virial and core radii of Coma are given by $R_{200} = 2.3 \text{ Mpc}$ ([Reiprich & Böhringer 2002](#)) and $R_c = 294 \text{ kpc}$, respectively. In accordance with Faraday rotation measure measurements, we assume $B(r) = B_0(n/n_0)^\eta$, where $B_0 = 4.8 \mu\text{G}$ and $\eta = 0.5$ ([Bonafede et al. 2010](#)).

The bulk of the CRps are injected by relatively low Mach number shocks and parametrized by $f_{\text{p,inj}}(p) = C_{\text{inj}} p^{-\alpha_{\text{inj}}}$, where $\alpha_{\text{inj}} \approx 2.5$ in our simulations. The CRps

approximately trace the thermal gas with $C_{\text{inj}} \propto \varepsilon_{\text{th}}^{\alpha_{\text{CR,spat}}}$ ([Pinzke & Pfrommer 2010](#); [Vazza et al. 2016](#)), where the normalisation is fixed by the injection rate of CR energy in the last 650 Myrs. Our simulations show that the CR energy approximately amounts to 0.03 per cent of the thermal energy inside the virial radius, i.e. $\int_0^{R_{200}} \varepsilon_{\text{CR,inj}} dV \left(\int_0^{R_{200}} \varepsilon_{\text{th}} dV \right)^{-1} = 0.0003$. The spectrum of the initial CRp distribution is determined by the steady state between injection and cooling,

$$f_{\text{p},0} \propto \frac{\int_p^\infty f_{\text{p,inj}}(p') dp'}{\left| \frac{dp}{dt} \right|_{\text{Coul}} + \frac{p}{\tau_{\text{had}}}}, \quad (26)$$

where we fix the normalisation by requiring $\int_0^{R_{200}} \varepsilon_{\text{CR},0} dV \left(\int_0^{R_{200}} \varepsilon_{\text{th}} dV \right)^{-1} = 0.003$. Note that the injected CR energy in the last 650 Myr is smaller by about a factor of 10 in comparison to the cumulative CR energy injected over the entire cosmological history of the cluster. However, since the injected CR energy rate averaged over the formation time of the cluster is similar to that during a merger, the CRes injected during the merger are especially important for the radio emission above 1 GHz since these CRs have not yet had time to cool. Similarly, the initial CRE distribution is given by the steady state between cooling (Coulomb, inverse Compton, and synchrotron) and injection of secondary CRes from $f_{\text{p},0}$. The diffusion constant $D_{pp} \propto X_{\text{tu}}^2 \varepsilon_{\text{th}}^{\alpha_{\text{tu}}-1} \sqrt{T} k_L$ is calculated for each radial bin. All parameters and assumptions are similar to what is used for our simulated cluster (see section 3). Our fiducial model assumes $X_{\text{tu}} = 0.2$, $\alpha_{\text{tu}} = 0.8$, $\alpha_{\text{CR,spat}} = 1.0$, and $k_L = 2\pi/\lambda_L$ where $\lambda_L = 100 \text{ kpc}$. We also assume a fixed acceleration time of $\tau_{\text{cl}} = 650$ Myr.

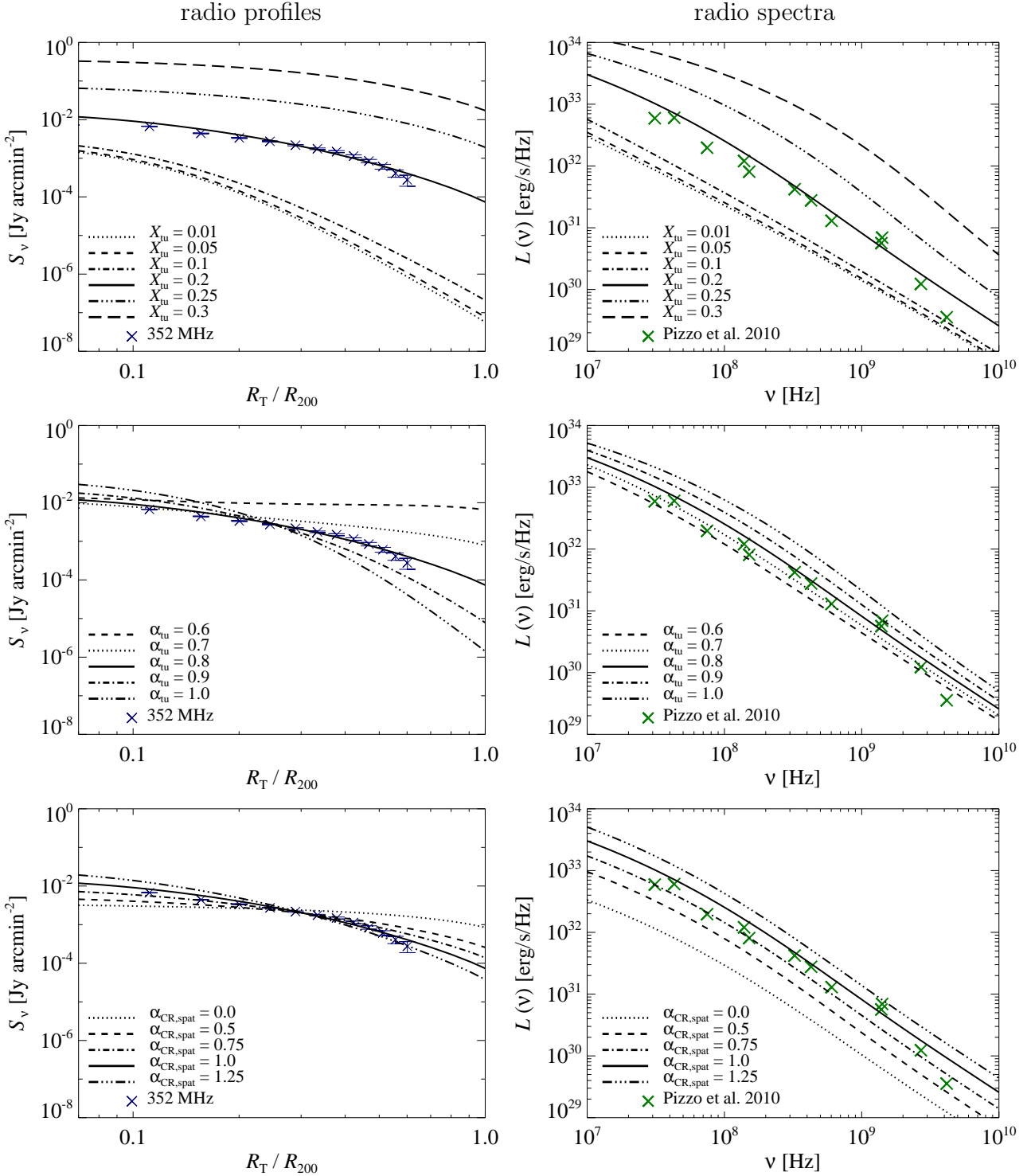


Figure 6. Sensitivity of the radio emission in the Coma cluster to critical parameters. The left-hand panels show the radio surface brightness profiles. We compare profiles at 352 MHz (blue crosses, [Brown & Rudnick 2011](#)) to predicted emission from Fermi-II reaccelerated CR electrons (black lines). The right-hand panels show radio synchrotron spectra. The green crosses are compiled from observations ([Pizzo 2010](#)), while the black lines show predicted spectra. The upper panels show the sensitivity to the level of turbulence (X_{tu}), the middle panels show the impact of different turbulent profiles (α_{tu}), and the lower panels show the dependence on spatial distributions of initial and injected CRs ($\alpha_{CR,spat}$). We adopt the following fiducial values for our model (solid lines), $X_{tu} = 0.2$, $\alpha_{tu} = 0.8$, and $\alpha_{CR,spat} = 1.0$ and vary each parameter separately in each row of panels. We find that the radio emission is most sensitive to the level of turbulence. The abundance of CR seeds, and the spatial distribution of CRs and turbulence are second-order effects.

4.2 Results

Figure 6 shows the impact of turbulence and the spatial distribution of CRs on the radio emission.

Impact of overall level of turbulence (X_{tu}). From the top panels of Figure 6, we see that as X_{tu} increases, there are 3 important changes: an exponential increase in radio luminosity, a flattening of the radio surface brightness profile, and an increase in spectral curvature. We discuss these in turn.

As we show in Section 4.3, the exponential increase in radio surface brightness is easily understood from equation 30, since for a power-law initial distribution function $f_i(p) = C_0 p^{-\alpha_{\text{inj}}}$, then $C_{\text{reacc}} \propto C_0 \exp(A\tau_{\text{cl}}/\tau_{\text{D}}) \propto \exp(B(r)X_{\text{tu}}^2)$. This exponential sensitivity is somewhat modified by cooling (which results in a non power-law spectrum; also, the shorter the acceleration time, the larger the pool of seed electrons available which would otherwise cool away), but overall is a good approximation.

An increase in X_{tu} flattens the surface brightness profile, since high acceleration efficiency leads to larger amplification in the cluster outskirts (where cooling is less important) than the centre. In particular, in the cluster outskirts, the reduced impact of Coulomb cooling implies that there is a larger pool of low-energy electrons available for reacceleration (see timescales in Table 1).

Larger levels of turbulence also *increase* spectral curvature, which might seem puzzling. It can be understood as follows. The pre-acceleration electron distribution function results from the competition between hadronic injection $f \propto p^{-\alpha_{\text{inj}}}$ and cooling, which results in a quasi-steady state for the non-thermal (secondary) electrons. At low momenta, when the Coulomb cooling time is short, $f \propto p^{-\alpha_{\text{inj}}+1}$, at high momenta, when inverse Compton/synchrotron cooling dominates, $f \propto p^{-\alpha_{\text{inj}}-1}$. In between, there is a quasi-adiabatic regime where electrons accumulate (for more details, and an analytic self-similar solution, see Sarazin 1999; Pinzke et al. 2013). In the absence of cooling, momentum advection in the limit $D_{pp} \propto p^2$ (so that $\tau_{\text{D}} = p^2/4D_{pp}$ is momentum independent) simply shifts the distribution $f(p) \rightarrow f(Ap)$. When the acceleration efficiency is low, most observable emission corresponds to the power-law tail of the distribution function $f \propto p^{-\alpha_{\text{inj}}-1}$ set by the balance between injection and synchrotron/IC cooling. However, as the acceleration efficiency A increases, radio emission starts to probe the 'bump' around p_* (given by $\tau_{\text{D}} \sim \tau_{\text{cool}}(p_*)$) where electrons accumulate and the distribution function is curved. This results in a curved emission spectrum. The synchrotron spectrum steepens at the frequency (Brunetti et al. 2001):

$$\nu_s \propto \frac{B\tau_{\text{D}}^{-2}}{(B^2 + B_{\text{CMB}}^2)^2} \quad (27)$$

where $B_{\text{CMB}} \equiv (8\pi\epsilon_{\text{CMB}})^{1/2}$, which increases for shorter τ_{D} .

Impact of spatial profile of turbulence (α_{tu}). From the middle panels of Figure 6, we see that as expected, a flatter profile of the turbulent pressure directly translates into a flatter radio surface brightness profile. Since seed electrons are more concentrated toward the centre (the collisional production of secondaries is more rapid there), and magnetic fields are stronger, concentrating the turbulence toward the cluster centre for fixed X_{tu} results in higher radio luminosities, and slightly more curvature (due to the increased im-

portance of cooling near the centre). Overall, however, the spatial profile of turbulence has a much weaker effect than its overall normalisation.

Impact of spatial profile of seed CRs $\alpha_{\text{CR,spat}}$. The spatial distribution of CRs has an even smaller impact on radio emission. At fixed total CR energy content X_{CR} , concentrating the CRs towards the centre leads to more centrally dominated surface brightness profiles, as expected, and higher radio luminosities (for the same reasons as above: secondaries are more easily produced in the centre, and magnetic fields are stronger). We have also confirmed that radio surface brightness profiles scale linearly with X_{CR} , as expected.

Overall, our results suggest that radio haloes are much more sensitive to the level of turbulence (exponential dependence) rather than CR abundance (linear dependence), and that the spatial distribution of turbulence and CRs, while important, are second-order effects. In our parametrization, the most important controlling variable is X_{tu} . The overall level of turbulence has to be such that $\tau_{\text{D}} \sim \tau_{\text{cl}}$ (see Table 1), otherwise, too little or too much amplification takes place. For instance, for $X_{\text{tu}} \gtrsim 0.08$, changing X_{tu} by a factor of two changes the radio surface brightness by a factor of $\sim 10 - 100$ (see top panels of Figure 6). The required $\tau_{\text{D}}/\tau_{\text{cl}}$ depends only logarithmically on the abundance of seed CRs.

While the requirement of a threshold level of turbulence may explain why radio brightness is bimodal, it also raises a fine-tuning problem: why is the L_{radio} vs. L_X relation in active radio haloes so tight (Brunetti et al. 2009)? Depending on the details of infall or mergers, we would naturally expect fluctuations in X_{tu} , which would translate into large scatter in the $L_{\text{radio}}-L_X$ relation. This can be only be understood if the timescale over which acceleration takes place τ_{cl} also depends on the properties of turbulence, so that the ratio $\tau_{\text{D}}/\tau_{\text{cl}}$ has relatively little scatter. We address this next.

4.3 Self-limiting turbulent reacceleration

In this section, we explore the physical origin of the high sensitivity of radio emission to turbulence levels (e.g., top right panel of Fig. 6), which thus requires strong fine-tuning to explain observed radio profiles. We will find that by relating the acceleration time to the turbulent decay time, this sensitivity can be eliminated. We also challenge the common assumption of assuming a Kraichnan spectrum, beginning at the outer scale (see Section 2.2). Since turbulence is essentially hydrodynamic at large scales, this is unjustified. Instead, we shall assume that the outer scale of the compressive fast modes is the Alfvén scale.

There are 3 important timescales in this problem: the acceleration time τ_{D} , the duration over which turbulence is active and acceleration takes place, τ_{cl} , and the cooling time $\tau_{\text{cool}}(p)$. Only $\tau_{\text{cool}}(p)$ is momentum dependent (and is different for ions and electrons). Thus, the outcome of acceleration depends essentially on two dimensionless numbers, $\tau_{\text{cl}}/\tau_{\text{D}}$, and $\tau_{\text{cool}}/\tau_{\text{D}}$.

We have seen that the radio luminosity depends very sensitively on $\tau_{\text{cl}}/\tau_{\text{D}}$, through the very sensitive dependence on X_{tu} (Figure 6; note from equation (15) that $\tau_{\text{D}} \propto X_{\text{tu}}^{-2}$). Since this raises questions of fine-tuning in X_{tu} to explain the observations, it is worth understanding this property in more detail. To this end, we ignore cooling, which is a good

approximation for the CR protons, because hadronic cooling times are long in comparison to the other relevant timescales of the problem.⁵ In this case, $\dot{p} = p/\tau_D$, and after a time τ_{cl} , we have

$$p \rightarrow p \exp(\tau_{cl}/\tau_D) \quad (28)$$

(where we have used the fact that τ_D is momentum independent). For an initial power law distribution function $f(p) = Cp^{-\alpha_{inj}}$, this momentum increase can be rewritten as a change of normalisation, $f(p) = \tilde{C}p^{-\alpha_{inj}}$, where $\tilde{C} = \exp(\alpha_{inj}\tau_{cl}/\tau_D)$. A slightly more careful derivation by direct solution of the Fokker-Planck equation yields:

$$\dot{f} = \frac{\partial}{\partial p} p^2 D_{pp} \frac{\partial f}{\partial p} \frac{f}{p^2}, \quad (29)$$

with the analytic solution given by

$$\tilde{C} = C \exp\left[\frac{(2 + \alpha_{inj})(\alpha_{inj} - 1)}{4} \frac{t}{\tau_D}\right]. \quad (30)$$

At $t = \tau_{cl}$ the CR distribution is exponentially sensitive to τ_{cl}/τ_D , which is the physical reason underlying the extreme sensitivity to X_{tu} in Figure 6.

The natural solution to this puzzle would be a process that couples τ_{cl} and τ_D . There are two possible limits. Let us suppose that the timescale on which there exists a source of turbulent driving is τ_{drive} , which approximately corresponds to the timescale of the merger, or the dynamical time. Let the turbulence decay on a timescale τ_{decay} . If $\tau_{drive} > \tau_{decay}$, then $\tau_{cl} \sim \tau_{drive}$, which depends on the details of the merger and should result in considerable scatter in τ_{cl}/τ_D in different systems. On the other hand, if $\tau_{decay} > \tau_{drive}$, then $\tau_{cl} \sim \tau_{decay}$. Since τ_D and τ_{decay} are both related to properties of the turbulence, it is conceivable that this would result in much less scatter in τ_{cl}/τ_D .

An obvious candidate for τ_{decay} is:

$$\tau_{edd} = \frac{L}{v_L} \quad (31)$$

i.e., the eddy turnover time at the outer scale. This is subject to uncertainties about the location of the outer scale L ; estimates in the literature range from $L \sim 0.1 - 1$ Mpc. It is also worth remembering that MHD turbulence only applies for $l < l_A$, where l_A is the Alfvén scale where $v \sim v_A$. Invoking fast modes, Kraichnan scalings, etc., is only valid below these scales. For $l > l_A$, turbulence is basically hydrodynamic.

In the hydrodynamic regime, a standard Hodge-Helmholtz decomposition usually shows that the compressive component of the velocity field is Burgers-like ($W(k) \propto k^{-2}$), while the solenoidal component is Kolmogorov-like ($W(k) \propto k^{-5/3}$), see e.g., Federrath (2013). The Burgers-like component does not reflect a genuine cascade, but rather the appearance of shocks which directly transfer power from large to small scales. At face value, we should use the Burgers spectrum for compressible modes. However, as already found by previous authors (Miniati 2015; Brunetti & Lazarian 2016), and as we shall discuss, this does not produce significant particle acceleration. If this is

the correct spectrum, then the paradigm of turbulent particle acceleration is simply flawed, and some other mechanism is necessary to explain radio halos. Alternatively, it is well-known that due to mode-mode coupling, solenoidal modes can give rise to compressive modes, and vice-versa (Kida & Orszag 1990; Cho & Lazarian 2003; Kritsuk et al. 2007), even for subsonic turbulence, since pressure fluctuations of order $\sim \rho u^2$ arise. Indeed, note that many numerical studies (such as Cho & Lazarian (2003); Kritsuk et al. (2007)) only have solenoidal driving on the outer scale, but then are also able to study the compressive modes that develop. In hydrodynamic turbulence, the energy in compressible modes which develop in this way scales as $\sim \mathcal{M}_s^2$, for $\mathcal{M}_s < 1$; this coupling is strongest at the Alfvén scale (Cho & Lazarian 2003). In MHD turbulence, mode-mode coupling is weak below the Alfvén scale and the Alfvén, fast and slow modes proceed as separate cascades.

We thus assume that some fraction of the Kolmogorov-like hydrodynamic turbulence which cascades down to the Alfvén scale ends up as compressive fast modes with a Kraichnan spectrum, as seen in simulations (Cho & Lazarian 2003). Henceforth, we can consider the outer scale of the fast modes to be l_A . If some fraction f_c of the turbulent energy density at this scale is in compressible modes, then the energy density at the outer scale is $\sim f_c \rho v_A^2$. The turbulent reacceleration time is:

$$\tau_D = \frac{p^2}{4D_{pp}} = \frac{C_D}{A^{1/2}} \frac{c}{k_A} \frac{\beta}{f_c v_A^2} \quad (32)$$

where $C_D = 2/(5\pi)$, $A \approx 11000$, and we have used equations, (6), (7), (14), assuming $s = 3/2$. The turbulent decay time is given by the cascade time of fast modes at the Alfvén scale $k = k_A$ (Yan & Lazarian 2004; see equation 11):

$$\tau_{decay} = \frac{v_{ph}}{v_k^2 k} = \frac{c_s}{f_c v_A^2 k_A} \quad (33)$$

This can be related to the eddy turnover time at the outer scale τ_{edd} from $l_A = LM_A^{-3}$ to:

$$\tau_{decay} = \frac{L}{v_L} \frac{c_s^2}{f_c v_L^2 c_s} \frac{v_A}{c_s} \approx 1.0 \tau_{edd} \left(\frac{\tilde{X}_{tu}}{0.2}\right)^{-1} \left(\frac{\beta}{50}\right)^{-1/2} \quad (34)$$

where we have used $\tilde{X}_{tu} \approx f_c (v_L/c_s)^2$ and $c_s/v_A = \beta^{1/2}$. The decay time at the Alfvén scale is comparable (and could be larger, if f_c is smaller than we have assumed) to the eddy turnover time at the outer scale. Thus, it is appropriate to consider the latter as the decay time for the fast modes, rather than the cascade time at the driving scale. The reason for these comparable timescales despite the disparate length scales is that large scale hydrodynamic modes cascade on a single eddy turnover time, whereas small scale sub-Alfvénic MHD modes are in the weak turbulence limit, and require multiple wave-wave interactions for a mode to cascade.

From equations (32) and (33), we obtain:

$$\frac{\tau_{cl}}{\tau_D} \approx \frac{\tau_{decay}}{\tau_D} = \frac{A^{1/2}}{C_D} \frac{c_s}{c} \beta^{-1} = 0.1 \left(\frac{c_s}{1500 \text{ km s}^{-1}}\right) \left(\frac{\beta}{50}\right)^{-1} \quad (35)$$

Remarkably, this expression is independent of properties of the turbulence such as v_c , L , or l_A , and depends only on properties of the plasma (c_s, β). Ultimately, this arises because the timescale on which a fast mode wave transfers energy due

⁵ In principle, CRp can still lose energy via wave heating, at a rate $|v_A \cdot \nabla P_{CR}|$, but we assume CR streaming is suppressed during mergers, when they are spatially confined by scattering.

to wave particle interactions in second order Fermi acceleration, $\tau_p \sim [4k_p c(v_c/c)^2]^{-1}$, is closely related to the timescale on which it cascades due to wave-wave interactions, $\tau_w \sim c_s/(k_w v_c^2)$. This implies $\tau_w/\tau_p \sim 4(c_s/c)(l_w/l_p)$, where $l_w \sim l_A$ is the outer scale on which the fast mode cascade begins, and $l_p \sim (l_A l_{\text{cut}})^{1/2}$ is the characteristic wavelength for wave-particle interactions. For transit time damping and an outer scale of l_A , we have $l_{\text{cut}} \sim (m_e/m_p)l_A(c_s/v_A)^4$. We thus have $\tau_w/\tau_p \sim 4(c_s/c)(l_A/l_{\text{cut}})^{1/2} \sim 4(c_s/c)(m_p/m_e)^{1/2}\beta^{-1}$. More careful consideration of dimensionless factors boosts this estimate by an order of magnitude to give equation (35).

On the other hand, equation (35) points toward a pessimistic scenario where turbulent reacceleration with TTD on thermal particles is never effective. A key reason is that we assume Kraichnan turbulence only applies for $l < l_A$. There is then insufficient separation of scales: the cutoff scale $l_{\text{cut}} \sim 0.2\beta_{50}^2 l_A$. Although there is a fair large separation of scales between the outer driving scale L and $l_A = LM_A^{-3}$ (a factor of 30 – 1000 for $M_A \approx 3 - 10$; we have $M_A \sim (\tilde{X}_{\text{tu}}\beta)^{1/2} \sim 3.2$ for our fiducial assumptions), Kolmogorov turbulence, with its steeper spectrum, has more energy at large scales ($kW(k) \propto k^{-2/3}, k^{-1/2}$ for Kolmogorov and Kraichnan turbulence, respectively). This implies that the energy-weighted scales at which wave-particle interaction take place are larger in Kolmogorov turbulence, and thus that the wave-particle interaction rate is lower. If (as is frequently seen) we instead assume that Kraichnan turbulence begins at the outer scale L , with characteristic decay time Lc_s/v_c^2 , then we obtain a more palatable result:

$$\frac{\tau_{\text{cl}}}{\tau_{\text{D}}} \approx 0.8 \left(\frac{c_s}{1500 \text{ km s}^{-1}} \right) \left(\frac{\tilde{X}_{\text{tu}}}{0.2} \right). \quad (36)$$

This arises because the decay time is now $\sim M_A$ times longer, and the acceleration time is now $\sim M_A^{1/2}$ times shorter, boosting $\tau_{\text{cl}}/\tau_{\text{D}}$ by $\sim M_A^{3/2}$. However, as we have argued, turbulence in the hydrodynamic regime $l_A < l < L$ is Kolmogorov, not Kraichnan. Furthermore, if this scaling is correct, then this leaves us with the problematic exponential sensitivity to X_{tu} that we previously explored.

One alternative is that scattering in the high- β ICM is mediated by plasma instabilities (firehose, mirror) rather than Coulomb scattering. This vastly increases the scattering rate and reduces the mean free path of thermal particles. In this case, the fast modes damp by TTD on relativistic rather than thermal particles. The momentum diffusion coefficient in this case is then (Brunetti & Lazarian 2011; Miniati 2015):

$$D_{pp}^{\text{CR}} = \frac{2p^2\zeta}{X_{\text{CR}}} k_L \frac{\langle v_c^2 \rangle}{c_s^3} \quad (37)$$

where ζ is an efficiency factor for the effectiveness of plasma instabilities (e.g., due to spatial or temporal intermittency), and $X_{\text{CR}} = \epsilon_{\text{CR}}/\epsilon_{\text{th}}$ is the relative energy density of CRs. If we set $k_L \rightarrow k_A$, $v_c^2 \rightarrow v_A^2$, as before, then:

$$\frac{\tau_{\text{cl}}}{\tau_{\text{D}}} \approx 8 \frac{\zeta}{\beta X_{\text{CR}}} \quad (38)$$

In principle, this implies exponential sensitivity to X_{CR} , a similar situation as exponential sensitivity to X_{tu} . However, there is a self-limiting asymptotic behaviour: as X_{CR} increases due to turbulent reacceleration, damping increases, which limits the further growth of the CR energy density

(Brunetti & Lazarian 2011). One natural assumption is to assume that ϵ_{CR} saturates at a level $\epsilon_{\text{CR}} \sim \epsilon_{\text{turb}}(\text{MHD}) \sim \epsilon_{\text{B}}$, in which case $X_{\text{CR}} \sim \beta^{-1}$, so that:

$$\frac{\tau_{\text{cl}}}{\tau_{\text{D}}} \approx 2.5 \left(\frac{\zeta}{0.3} \right). \quad (39)$$

Given the host of uncertain factors which enter into $\zeta < 1$ (the intermittent nature of turbulence, small scale magnetic topology and the efficiency with which instabilities mediated by pressure anisotropies are triggered), this is potentially consistent with $\tau_{\text{cl}} \sim \tau_{\text{D}}$. This promising scenario should be investigated in more detail.

It is also worth exploring the effect of Burgers' turbulence (weak shocks). Burgers' turbulence is distinct from other forms of turbulence in that it violates locality in k -space—i.e., power does not gradually cascade, but instead can directly jump from large to small scales via a network of weak shocks. This implies a short dissipation time and we have in this case, $\tau_{\text{cl}} \sim \tau_{\text{drive}}$, the driving time, rather than the turbulent dissipation time. Since the Fourier transform of a step function goes as k^{-1} , Burgers turbulence has a power spectrum of $P(k) \propto k^{-2}$. From equations (6) and (7), we find:

$$\frac{D_{pp}^{\text{Burgers}}}{D_{pp}^{\text{MHD}}} = \left(\frac{\beta}{X_{\text{tu}}A} \right)^{1/2} = 0.15 \left(\frac{\beta}{50} \right)^{1/2} \left(\frac{X_{\text{tu}}}{0.2} \right)^{-1/2} \quad (40)$$

where we have set $\langle k \rangle_{\text{W}} \approx k_L$ for Burgers' turbulence, i.e. all power is at large scales. This weighting towards larger scales implies a much lower wave-particle interaction rate and thus a diffusion coefficient which is smaller than standard TTD on thermal particles by an order of magnitude. Since $\langle k \rangle_{\text{W}} \approx k_L$ is independent of the cutoff scale k_{cut} , this conclusion is unchanged if plasma instabilities regulate the thermal particle mean free path and TTD operates on relativistic particles instead. Since standard TTD on thermal particles was already potentially problematic (equation 35), we conclude, in agreement with other assessments (Miniati 2015; Brunetti 2016), that if Burgers turbulence dominates, then turbulent reacceleration will be ineffective.

It is interesting to reconsider surface brightness and spectral profiles if indeed $\tau_{\text{D}} \sim \tau_{\text{cl}}$ for the reasons mentioned above (e.g., equation 39). We show the results of adopting such an ansatz in Figure 7, where, similar to Figure 6, we vary X_{tu} , α_{tu} , and $\alpha_{\text{CR,spat}}$ about fiducial values.⁶ Instead of adopting a fixed τ_{cl} , we set $\tau_{\text{cl}}/\tau_{\text{D}} = 2.5$. The results are remarkably revealing. In this case, we are indeed less sensitive to the properties of the turbulence, and more sensitive to the details of the CR seed population. This gives hope to the possibility that one could effectively marginalise over the very uncertain properties of turbulence at larger scales in merging clusters (which are unlikely to be more precisely constrained observationally in the near future) to learn something about the underlying CR population.

For instance, in the third row of panels of Figure 7, we see that once turbulence exceeds a threshold value $X_{\text{tu}} \sim 0.2$,

⁶ When $\tau_{\text{cl}}/\tau_{\text{decay}} \sim \text{const}$ is adopted, the radial behaviour of τ_{cl} is also modified. Because τ_{D} decreases with radius (see e.g. Figure 4), τ_{cl} has to decrease by the same amount, which results in a steeper radio profile. To compensate for this effect in Figure 7, we change $\alpha_{\text{CR,spat}} = 1.0 \rightarrow 0.5$ and decrease the injection rate of CR energy by a factor five.

then its overall exact energy density does not matter – profiles simply converge to an asymptotic form as X_{tu} is increased. This is in contrast to the exponential sensitivity, flattening in surface brightness, and increasing spectral curvature as X_{tu} is increased that we saw previously. A threshold value of X_{tu} is necessary for turbulent reacceleration to overcome cooling. Once that condition is satisfied, the condition $\tau_{\text{cl}}/\tau_{\text{D}} \sim \text{const}$ implies a fixed amount of amplification: stronger turbulence implies faster acceleration, but also dissipates more quickly. This leads to the asymptotic behaviour seen. The value of this constant depends on plasma physics details, but we have shown that the value required to match observations is plausible.

The second row of panels of Figure 7 reveal another striking result: in contrast to Figure 6, results are also completely insensitive to the spatial profile of turbulence. Given the large uncertainties, this is a welcome property. It arises because for our fiducial value ($X_{\text{tu}} = 0.2$), variations in the turbulent profile still lead to local energy densities which are above the threshold value required to overcome cooling, and turbulent amplification approaches its asymptotic value.

Finally, in the top panels of Figure 7, we see that we *are* sensitive to the spatial profile of CRs; it affects both the radio surface brightness profile (a flatter CR distribution implies flatter surface brightness profiles) and luminosity (once again, luminosity is larger for more centrally concentrated CRs, since more secondaries are produced). This arises because once turbulent reacceleration overcomes cooling, the condition $\tau_{\text{cl}}/\tau_{\text{D}} \sim \text{const}$ provides a fixed amount of amplification in each radial shell. The radio luminosity in each shell then depends linearly on initial conditions, i.e., the profile of CR seeds. Interestingly, the best-fitting profile for Coma results from a flat CR distribution – i.e., the outcome of efficient CR streaming. The overall amplitude is set by $\tau_{\text{cl}}/\tau_{\text{D}}$ (equation 39) and the CR content.

Obviously, the ideas in this section require further study. For instance, the notion that fast modes appear abruptly at I_{A} and that they last for a time τ_{cl} are clear approximations (the latter could be improved by solving the time dependent diffusion equation for the fast mode energy spectrum, see e.g. Zhou & Matthaeus (1990)). However, the notion that $\tau_{\text{cl}}/\tau_{\text{D}}$ could self-regulate around a fixed value is exciting, because it eliminates the main source of uncertainty – the poorly unconstrained properties of turbulence, and implies that radio haloes could potentially provide more robust constraints on the underlying CR population.

5 CONCLUSIONS

The standard reacceleration model for radio haloes requires two ingredients with no current direct observational constraints: a CR population which produces seed electrons, and turbulence to perform second-order Fermi acceleration on these electrons⁷. For the best studied radio halo, Coma, there are two main observational constraints: the radio surface brightness profile $S_{\nu}(r)$, and the integrated luminosity as a function of frequency $L(\nu)$. For certain assumptions about

turbulence and the seed population, analytic theoretical models can match these observations (Brunetti & Lazarian 2011), but the realism of the assumed seed electron and turbulent profiles must be confronted with numerical simulations.

Cluster turbulence has been studied numerically in cosmological simulations with an eye toward radio halo properties (Beresnyak et al. 2013; Miniati 2015), though they were not confronted against the two benchmark observations mentioned above. Most importantly, direct simulation of the seed electron population has been missing in the literature. In this paper, we fill that gap. At the same time, we study the sensitivity of radio halo profiles and spectra to variation in properties of turbulence and seed population, and uncover the dominant effects.

In the first part of the paper, we use hydrodynamic zoom simulations of a Coma-like cluster in a cosmological setting to generate spatially and momentum-resolved seed populations of CRps and CRe from diffusive shock acceleration. The simulations include time-dependent cooling and adiabatic transport processes, and has been previously used in a variety of applications in CR cluster physics (Pinzke & Pfrommer 2010; Pinzke et al. 2013). The resultant CRp and CRe distribution functions then serve as initial conditions for our calculations of Fermi II acceleration by turbulence. We use time-dependent Fokker-Planck calculations which allow for spatial variations in the properties of turbulence (i.e., a spatially varying momentum diffusion coefficient). We adopt a simple parametric model for cluster turbulence, characterising it by its overall normalisation, spatial profile, and characteristic lifetime τ_{cl} . Our approach is relatively sophisticated in its treatment of the CR seed population and relatively simplified in its treatment of the turbulence; it is thus orthogonal and complementary to existing treatments which focus on the time-dependent compressible turbulence (Miniati 2015).

Given our seed electron population (which includes both primaries generated by DSA and secondary electrons created by CRps in hadronic interactions; for standard assumptions, the latter dominates), we find that applying the standard model previously used to reproduce Coma’s radio halo properties (Brunetti & Lazarian 2011), in which $\varepsilon_{\text{turb}} \propto \varepsilon_{\text{th}}$, fails: it produces radio emission which is too centrally concentrated. Indeed, Brunetti & Lazarian (2011) remark in their paper that the CR population required in their model is remarkably flat. By contrast, the simulations produce CRs which are more centrally concentrated.

Thus, some modification of the standard model is needed, either by modifying the spatial distribution of the CRs, or that of turbulence. We explore two examples of the former: (i) CRs can stream in the ICM, producing a flat profile (Enßlin et al. 2011; Wiener et al. 2013), or (ii) given a higher e/p ratio in DSA acceleration (perhaps due to magnetic geometry; Guo et al. 2014a), the primary population can dominate. This has a much flatter profile (since secondaries must be generated collisionally, they will always be concentrated towards denser regions). However, both of these solutions still require some modification of the turbulent profile, requiring $\varepsilon_{\text{turb}}/\varepsilon_{\text{th}}$ to rise with radius. Indeed, one can simply use the unmodified CR profile derived from simulations if (iii) $\varepsilon_{\text{turb}}/\varepsilon_{\text{th}}$ rises somewhat more steeply with radius. The fact that $\varepsilon_{\text{turb}}/\varepsilon_{\text{th}}$ rises with radius is well sup-

⁷ Other model ingredients, such as temperature, density, and B-field profiles, are observationally constrained by X-ray and Faraday rotation measurements.

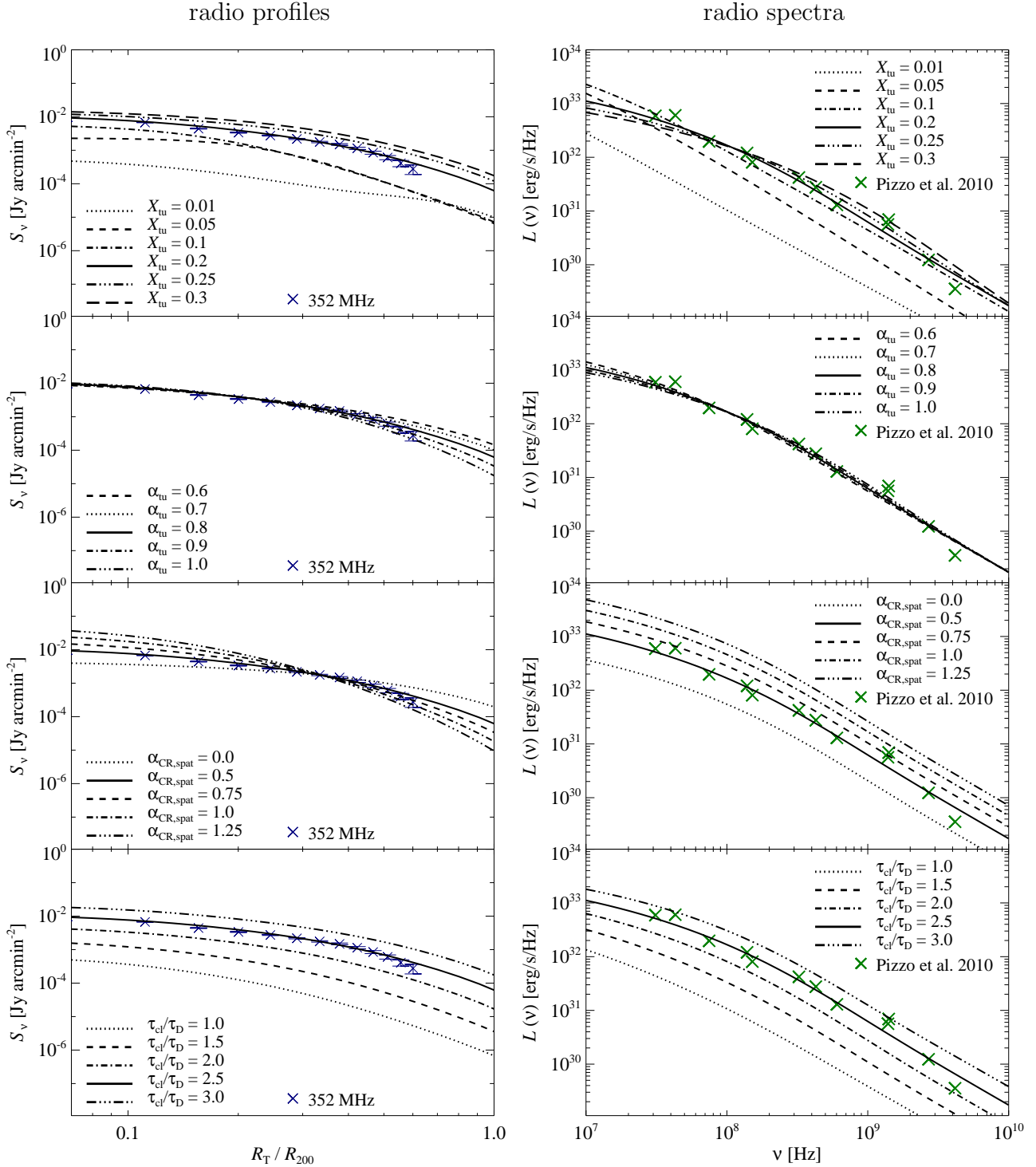


Figure 7. Sensitivity of radio emission in the Coma cluster to critical parameters when we vary the ratio of the time scales on which turbulence is active (τ_{cl}) to the turbulent re-acceleration time (τ_D). In comparison to Figure 6, we change our fiducial model (solid lines) and adopt a slightly more extended spatial distribution of CRs ($\alpha_{CR,spat} = 0.5$) and lower the injection rate of CR energy by a factor five; otherwise, we adopt $X_{tu} = 0.2$, $\alpha_{tu} = 0.8$, $\tau_{cl} = 2.5 \tau_D$ as fiducial values and vary each parameter separately in each row of panels. Radio surface brightness profiles (left) are contrasted to radio synchrotron spectra (right; for more details see caption to Figure 6). Provided there is a minimum (threshold) level of turbulence ($X_{tu} \gtrsim 0.2$), here the radio profiles are mainly determined by the CR distribution, while turbulence has a remarkably small impact. In the bottom two panels we vary the exponential momentum growth factor τ_{cl}/τ_D (see equations 28 and 30), which mainly changes the normalisation of the CR distribution and neither spectral shape nor radial synchrotron profile. Interestingly, the flat CR profiles adopted here are similar to those required to reproduce the radio profiles in our CR streaming model (see Figure 2).

ported by cosmological hydrodynamic simulations of clusters (Lau et al. 2009; Shaw et al. 2010; Vazza et al. 2011a); even the last model (iii) is (within the scatter) perfectly consistent with the trends seen by such simulations. This strongly suggests that a rising $\varepsilon_{\text{turb}}/\varepsilon_{\text{th}}$ should be part of any final model of radio haloes. Given the lack of observational constraints on turbulent profiles, this unfortunately means that models will have yet another degree of freedom.

The above models are merely meant to serve as existence proofs, showing what modifications to the standard model are necessary to be reconciled with the radio halo observations. There are too many uncertainties and parameter degeneracies for any of these models to be definitive, or for one to make firm quantitative statements about turbulent and seed CR profiles, apart from placing certain bounds. We abstract the main parameter dependencies by exploring static, spherically symmetric models consistent with Coma, where we repeat our Fokker-Planck calculations. We explore three main effects: the overall normalisation of turbulence, and spatial distribution of turbulence and CRs.

We find that the most important variable is the overall normalisation of turbulence: surface brightness scales exponentially with the amount of turbulence. The radio spectrum also becomes more curved with higher turbulence. In contrast, the surface brightness scales linearly with the CR abundance. The spatial distributions of both turbulence and CRs also influence radio halo profiles (for both, flatter distributions at fixed overall normalisation imply flatter surface brightness profiles with lower overall radio luminosity), but play a secondary role.

This exponential dependence of radio halo luminosity with turbulence then raises the interesting question of why radio halo scaling relations (e.g., L_V-L_X) are so tight. Previous statistical modelling of radio halo populations (Cassano et al. 2006, 2007) have focused on matching the mean relations, but not the scatter. We believe the latter provides a particularly interesting and potentially fruitful constraint. The acceleration timescale τ_D and the length of time during which acceleration takes place τ_{cl} must be matched so that there are roughly ~ 2 e-folds (given the factor ~ 10 difference in radio luminosity between the radio bright and faint populations; Brown & Rudnick (2011)), otherwise scatter in turbulence (which we might expect given the wide variety of merger and infall conditions) will be exponentially amplified in radio luminosity. The timescale of the merger has some natural scatter which is not obviously correlated with τ_D .

If instead we adopt $\tau_{\text{cl}}/\tau_{\text{decay}} \sim \text{const}$, i.e. the natural lifetime of turbulence is its decay lifetime, then we can show that the acceleration time and the lifetime of turbulence are coupled, simply because the wave-particle interaction rate (which drives particle acceleration) and the wave-wave interaction rate (which drives dissipation) are linked. If we are mindful that Kraichnan turbulence is only applicable below the Alfvén scale l_A (where turbulent velocities $v < v_A$), then remarkably the ratio τ_{cl}/τ_D is independent of properties of the turbulence (such as its amplitude and outer scale) and only depends on plasma parameters. Our results suggest that TTD on thermal particles may result in overly rapid damping of turbulence, and inefficient acceleration (equation 35), but if plasma instabilities scatter the thermal particles so that the fast modes damp via

TTD on the CRs, then the required acceleration can take place (equation 39). In agreement with other assessments, we find that if turbulence is Burgers rather than Kraichnan, then turbulent reacceleration is ineffective, and some other explanation for radio haloes (e.g., magnetic reconnection, Brunetti & Lazarian 2016) is necessary. If we adopt the ansatz $\tau_{\text{cl}}/\tau_{\text{decay}} \sim \text{const}$, then we find that above a threshold level of turbulence (necessary to overcome cooling), radio properties are insensitive to both the amplitude and spatial profile of turbulence, since only a fixed, asymptotic amount of amplification takes place. On the other hand, they are sensitive to the properties of the seed electron profile. This raises the exciting possibility that one could marginalise over the highly uncertain properties of cluster turbulence to learn about the underlying seed CR population. Our results suggest that studying not just mean trends, but the relatively small scatter in radio-halo scaling relations, may prove extremely fruitful in shedding light on ICM plasma processes.

Acknowledgements. We thank Josh Wiener for discussions on CR streaming, Lawrence Rudnick for discussion on uncertainties in the 1.4 GHz radio data, Fabio Zandanel for re-calculating gamma-ray limits, and Gianfranco Brunetti for useful discussions. We thank an anonymous referee for helpful comments that improved the paper. A.P. is grateful to the Swedish research council for financial support. S.P.O. thanks NASA grants NNX12AG73G and NNX15AK81G for support, as well as KITP for hospitality. This research was supported in part by the National Science Foundation under Grant No. NSF PHY11-25915. C.P. acknowledges support by the European Research Council under ERC-CoG grant CRAGSMAN-646955 and by the Klaus Tschira Foundation.

REFERENCES

- Ackermann M., et al., 2014, *ApJ*, **787**, 18
 Ahnen M. L., et al., 2016, *A&A*, **589**, A33
 Arlen T., et al., 2012, *ApJ*, **757**, 123
 Arnaud M., et al., 2001, *A&A*, **365**, L67
 Basu K., 2012, *MNRAS*, **421**, L112
 Beresnyak A., Xu H., Li H., Schlickeiser R., 2013, *ApJ*, **771**, 131
 Blasi P., Colafrancesco S., 1999, *Astroparticle Physics*, **12**, 169
 Bonafede A., Feretti L., Murgia M., Govoni F., Giovannini G., Dallacasa D., Dolag K., Taylor G. B., 2010, *A&A*, **513**, A30
 Bonamente M., Lieu R., Bulbul E., 2009, *ApJ*, **696**, 1886
 Briel U. G., Henry J. P., Boehringer H., 1992, *A&A*, **259**, L31
 Brown S., Rudnick L., 2011, *MNRAS*, **412**, 2
 Brunetti G., 2016, *Plasma Physics and Controlled Fusion*, **58**, 014011
 Brunetti G., Jones T. W., 2014, *International Journal of Modern Physics D*, **23**, 30007
 Brunetti G., Lazarian A., 2007, *MNRAS*, **378**, 245
 Brunetti G., Lazarian A., 2011, *MNRAS*, **412**, 817
 Brunetti G., Lazarian A., 2016, *MNRAS*, **458**, 2584
 Brunetti G., Setti G., Feretti L., Giovannini G., 2001, *MNRAS*, **320**, 365
 Brunetti G., Blasi P., Cassano R., Gabici S., 2004, *MNRAS*, **350**, 1174
 Brunetti G., Cassano R., Dolag K., Setti G., 2009, *A&A*, **507**, 661
 Brunetti G., Blasi P., Reimer O., Rudnick L., Bonafede A., Brown S., 2012, *MNRAS*, **426**, 956
 Caprioli D., Spitkovsky A., 2014, *ApJ*, **783**, 91
 Cassano R., Brunetti G., Setti G., 2006, *MNRAS*, **369**, 1577
 Cassano R., Brunetti G., Setti G., Govoni F., Dolag K., 2007, *MNRAS*, **378**, 1565
 Chernyshov D. O., Dogiel V. A., Ko C. M., 2012, *ApJ*, **759**, 113

- Cho J., Lazarian A., 2003, *MNRAS*, **345**, 325
- Deiss B. M., Reich W., Lesch H., Wielebinski R., 1997, *A&A*, **321**, 55
- Dennison B., 1980, *ApJ*, **239**, L93
- Dermer C. D., 1986, *ApJ*, **307**, 47
- Dolag K., Borgani S., Murante G., Springel V., 2009, *MNRAS*, **399**, 497
- Donnert J., Brunetti G., 2014, *MNRAS*, **443**, 3564
- Donnert J., Dolag K., Brunetti G., Cassano R., 2013, *MNRAS*, **429**, 3564
- Ellison D. C., Berezhko E. G., Baring M. G., 2000, *ApJ*, **540**, 292
- Enßlin T., Pfrommer C., Miniati F., Subramanian K., 2011, *A&A*, **527**, A99+
- Farmer A. J., Goldreich P., 2004, *ApJ*, **604**, 671
- Federrath C., 2013, *MNRAS*, **436**, 1245
- Feretti L., Giovannini G., Govoni F., Murgia M., 2012, *A&ARv*, **20**, 54
- Giovannini G., Feretti L., Venturi T., Kim K. T., Kronberg P. P., 1993, *ApJ*, **406**, 399
- Gould R. J., 1972, *Physica*, **60**, 145
- Govoni F., Enßlin T. A., Feretti L., Giovannini G., 2001, *A&A*, **369**, 441
- Guo X., Sironi L., Narayan R., 2014a, *ApJ*, **794**, 153
- Guo X., Sironi L., Narayan R., 2014b, *ApJ*, **797**, 47
- Kang H., Ryu D., 2011, *ApJ*, **734**, 18
- Kida S., Orszag S. A., 1990, *Journal of Scientific Computing*, **5**, 1
- Kowal G., Lazarian A., 2010, *ApJ*, **720**, 742
- Kritsuk A. G., Norman M. L., Padoan P., Wagner R., 2007, *ApJ*, **665**, 416
- Lau E. T., Kravtsov A. V., Nagai D., 2009, *ApJ*, **705**, 1129
- Lynn J. W., Quataert E., Chandran B. D. G., Parrish I. J., 2014, *ApJ*, **791**, 71
- Miniati F., 2015, *ApJ*, **800**, 60
- Miniati F., Ryu D., Kang H., Jones T. W., 2001a, *ApJ*, **559**, 59
- Miniati F., Jones T. W., Kang H., Ryu D., 2001b, *ApJ*, **562**, 233
- Park J., Caprioli D., Spitkovsky A., 2015, *Physical Review Letters*, **114**, 085003
- Petrosian V., East W. E., 2008, *ApJ*, **682**, 175
- Pfrommer C., 2008, *MNRAS*, **385**, 1242
- Pfrommer C., Enßlin T. A., 2004, *A&A*, **413**, 17
- Pfrommer C., Springel V., Enßlin T. A., Jubelgas M., 2006, *MNRAS*, **367**, 113
- Pfrommer C., Enßlin T. A., Springel V., Jubelgas M., Dolag K., 2007, *MNRAS*, **378**, 385
- Pfrommer C., Enßlin T. A., Springel V., 2008, *MNRAS*, **385**, 1211
- Pinzke A., Pfrommer C., 2010, *MNRAS*, **409**, 449
- Pinzke A., Oh S. P., Pfrommer C., 2013, *MNRAS*, **435**, 1061
- Pizzo R. F., 2010, PhD thesis, University of Groningen
- Planck Collaboration et al., 2013, *A&A*, **554**, A140
- Porter D. H., Jones T. W., Ryu D., 2015, *ApJ*, **810**, 93
- Quilis V., Ibanez J. M. A., Saez D., 1998, *ApJ*, **502**, 518
- Reiprich T. H., Böhringer H., 2002, *ApJ*, **567**, 716
- Rybicki G. B., Lightman A. P., 1979, *Radiative processes in astrophysics*. New York, Wiley-Interscience
- Sarazin C. L., 1999, *ApJ*, **520**, 529
- Sarkar S., Erlebacher G., Hussaini M. Y., Kreiss H. O., 1991, *Journal of Fluid Mechanics*, **227**, 473
- Schlickeiser R., Sievers A., Thiemann H., 1987, *A&A*, **182**, 21
- Shaw L. D., Nagai D., Bhattacharya S., Lau E. T., 2010, *ApJ*, **725**, 1452
- Subramanian K., Shukurov A., Haugen N. E. L., 2006, *MNRAS*, **366**, 1437
- Vazza F., Brüggén M., 2014, *MNRAS*, **437**, 2291
- Vazza F., Dolag K., Ryu D., Brunetti G., Gheller C., Kang H., Pfrommer C., 2011a, *MNRAS*, **418**, 960
- Vazza F., Brunetti G., Gheller C., Brunino R., Brüggén M., 2011b, *A&A*, **529**, A17
- Vazza F., Gheller C., Brüggén M., 2014, *MNRAS*, **439**, 2662
- Vazza F., Brüggén M., Wittor D., Gheller C., Eckert D., Stubbe M., 2016, *MNRAS*, **459**, 70
- Wiener J., Oh S. P., Guo F., 2013, *MNRAS*, **434**, 2209
- Yan H., Lazarian A., 2002, *Physical Review Letters*, **89**, 1102
- Yan H., Lazarian A., 2004, *ApJ*, **614**, 757
- Zandanel F., Ando S., 2014, *MNRAS*, **440**, 663
- Zandanel F., Pfrommer C., Prada F., 2014, *MNRAS*, **438**, 124
- Zhou Y., Matthaeus W. H., 1990, *J. Geophys. Res.*, **95**, 14881